Petrology of Sedimentary Rocks

G421P13, summer semester, 2/1 hours, 3-4th year

6. Geochemistry of sedimentary rocks, cathode luminiscence

Karel Martínek

Institute of Geology and Palaeontology

trace elements

B, Ba – Boron or Barium in clay minerals as an paleosalinity indicator

Zr, Ti, Ti/Al – proxies for terrestrial input and altered alkaline basic volcanism; Vanadium or other could be used for discrimination of terrigenous and volcanogenic Ti, V usually correlates with Ti in volcanogenic rocks

Rb – proxy for clay

Ba, Pb – proxy for feldspars

.....

environmental magnetism

Fe minerals – proxy of terrestrial input, weathering intensity (magnetite, hematite, limonite, sulphides, ... could be distinguished)

stable isotopes

$$\delta^{18}O\ [‰] = ((^{18}O/^{16}O_{sample} - ^{18}O/^{18}O_{SMOW})/\ ^{18}O/^{18}O_{SMOW})*1000$$

$$\delta^{13}C\ [‰] = ((^{13}C\ /^{12}C_{sample} - ^{13}C\ /^{12}C_{PDB})/\ ^{13}C\ /^{12}C_{PDB})*1000$$

SMOW, PDB – standards

isotopic fracionation processes in hydrosphere – changes of isotopic composition of water with temperature, lattitude, →ice stratigraphy

carbon cycle

carbonate systems, stratigraphy of pelagic carbonates, record of temperature and climatic changes

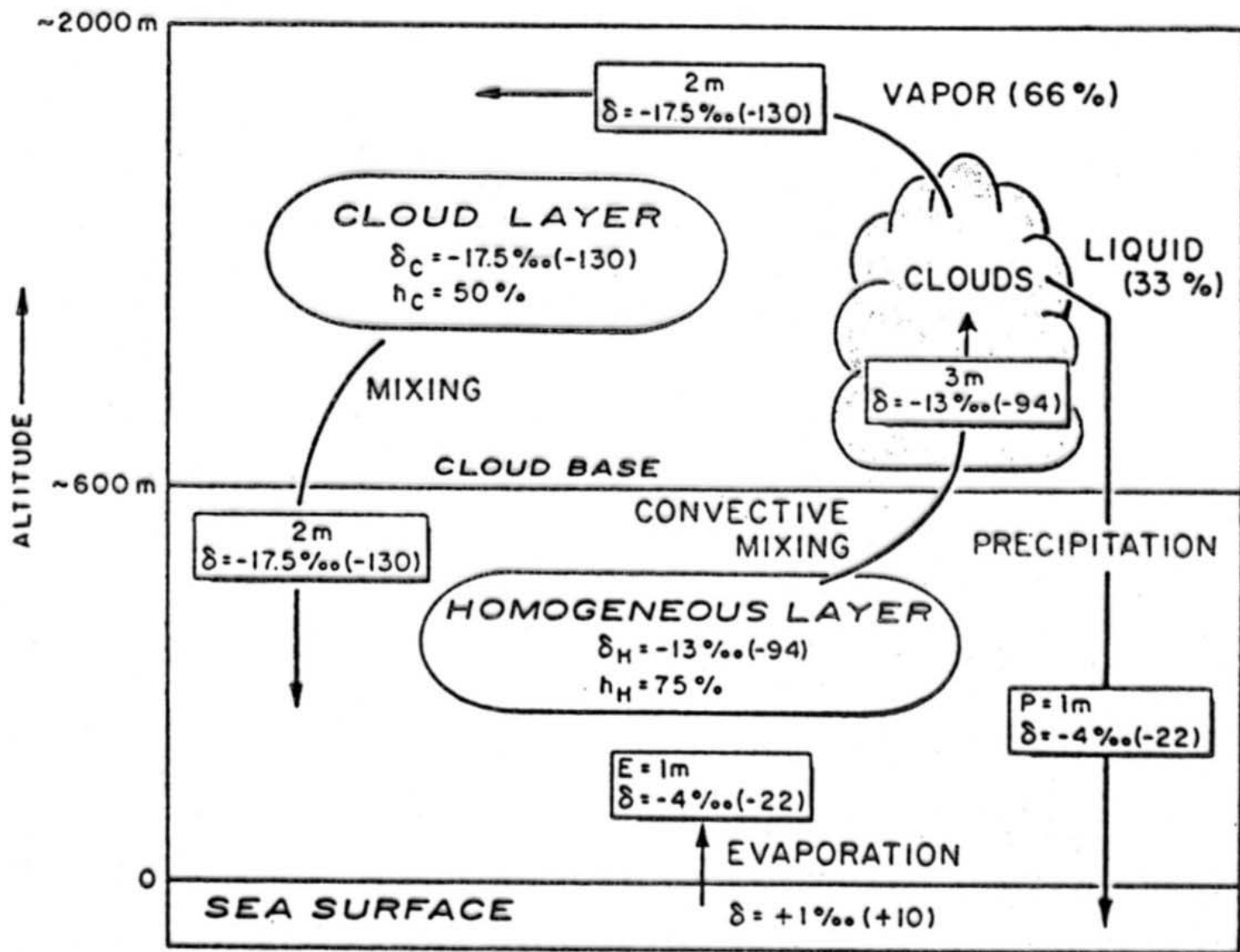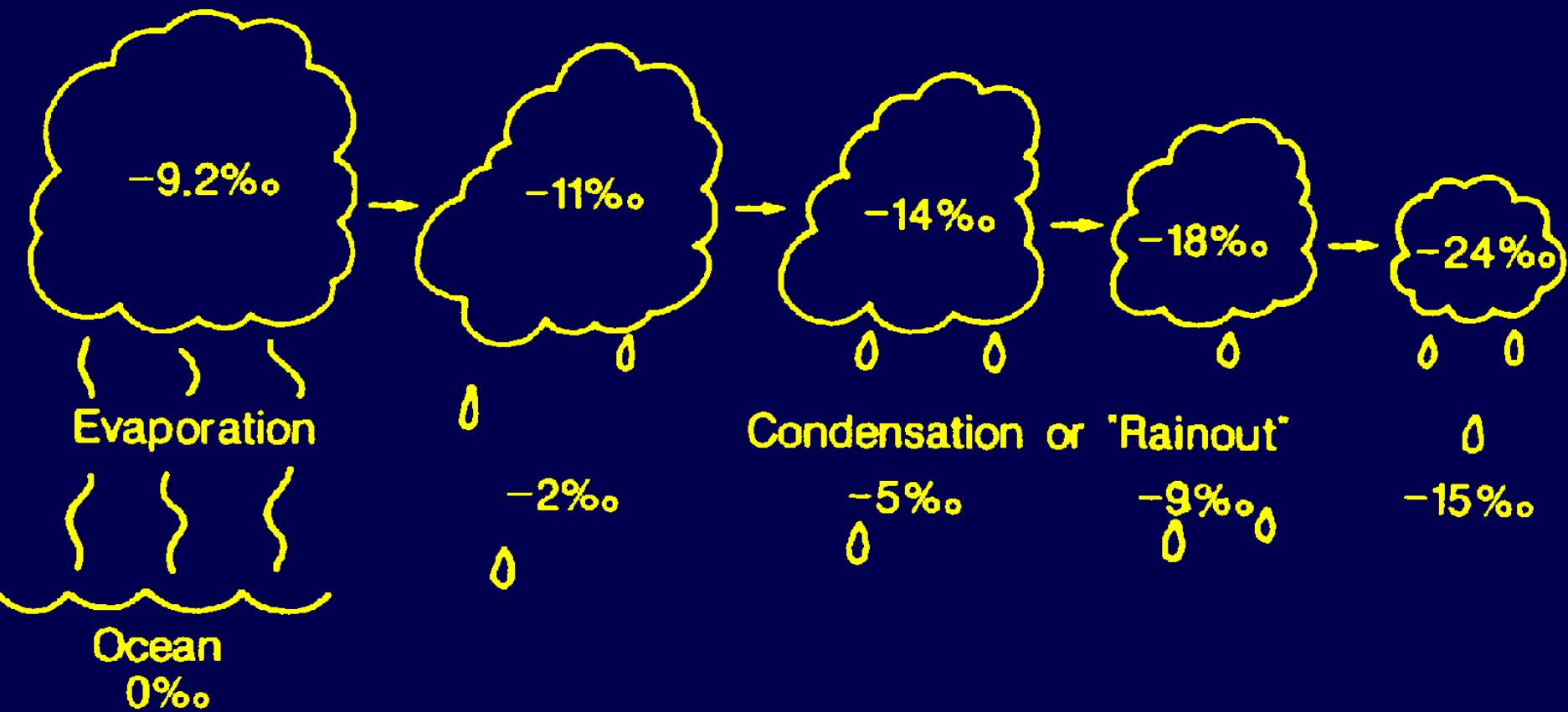$\delta^{13}C$ organic matter – types of metabolism of aquatic and terrestrial plants

Fig. 1-9. Stable isotope composition of the marine atmosphere (from Craig and Gordon, 1965). δ-values are given for ^{18}O and, in parentheses, for deuterium.
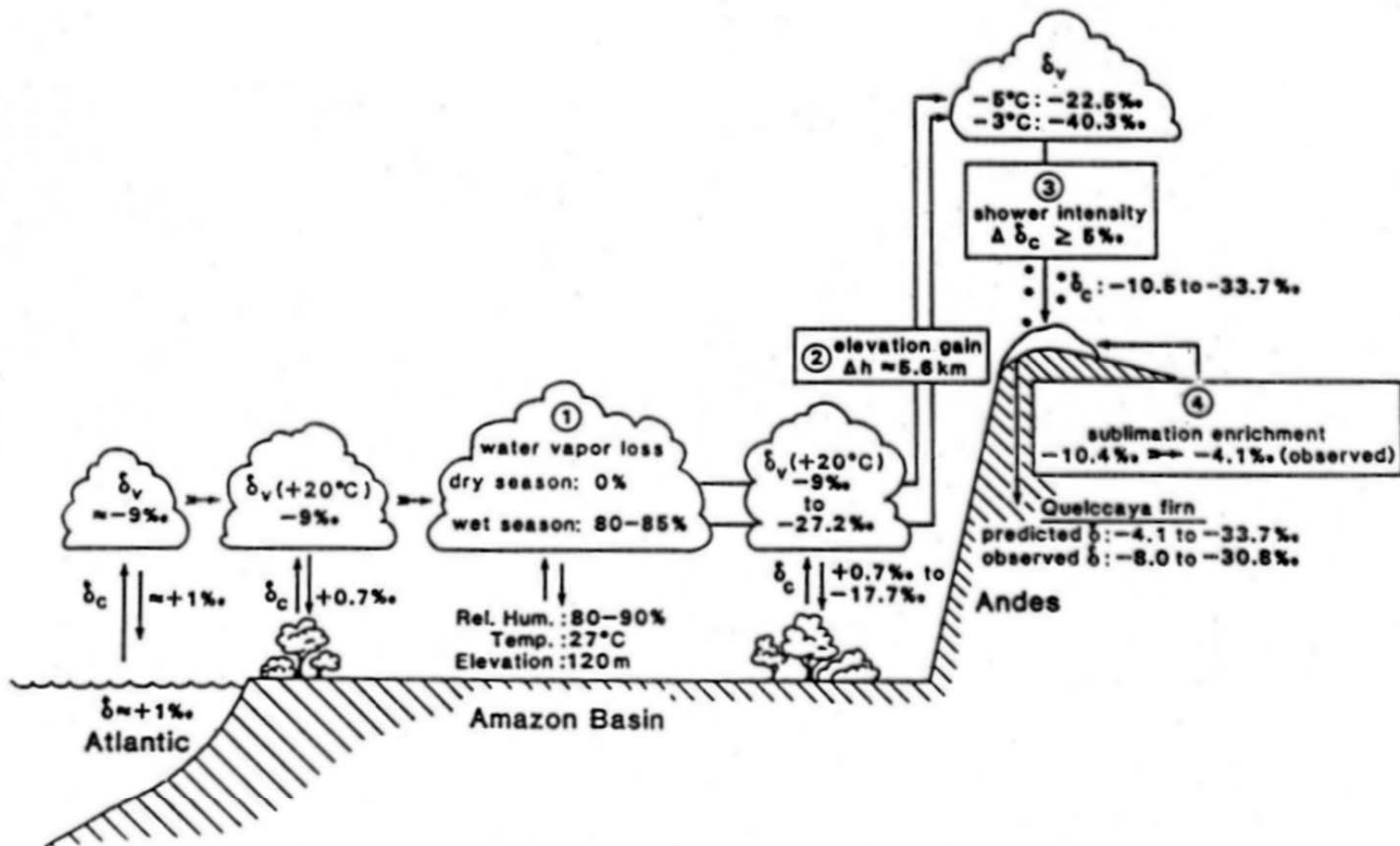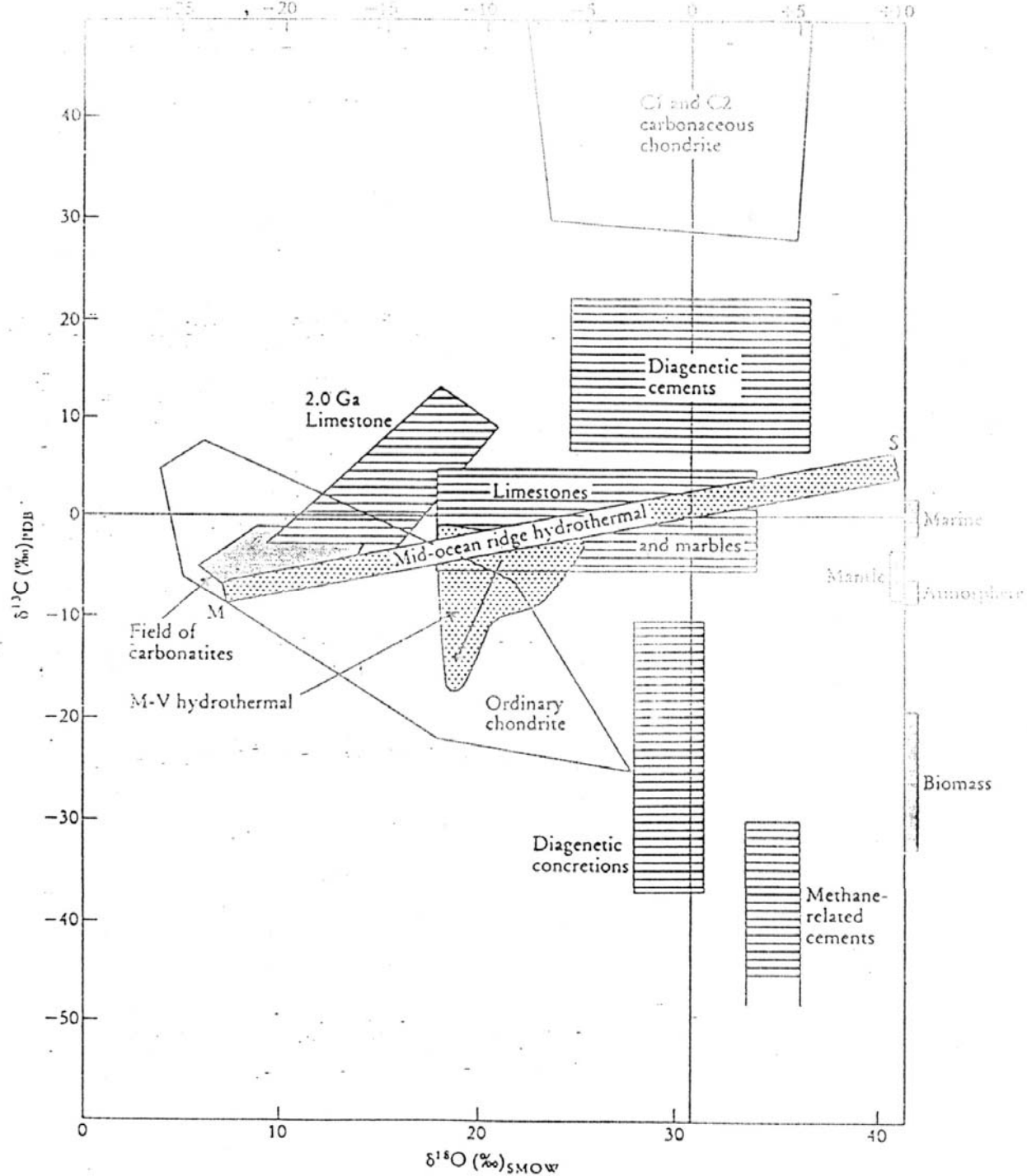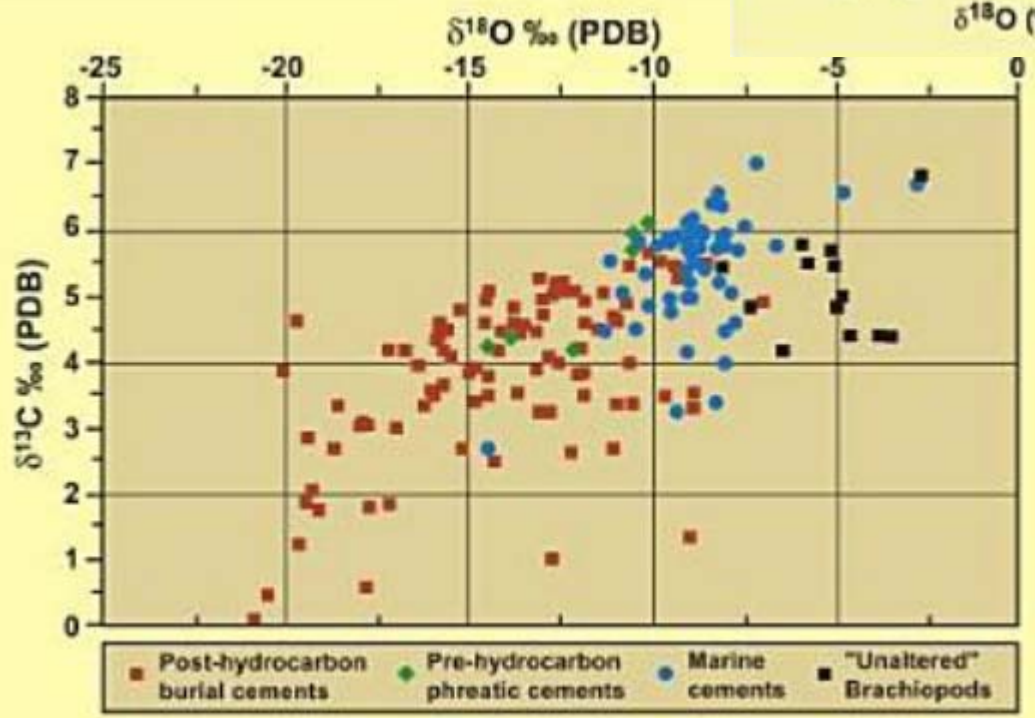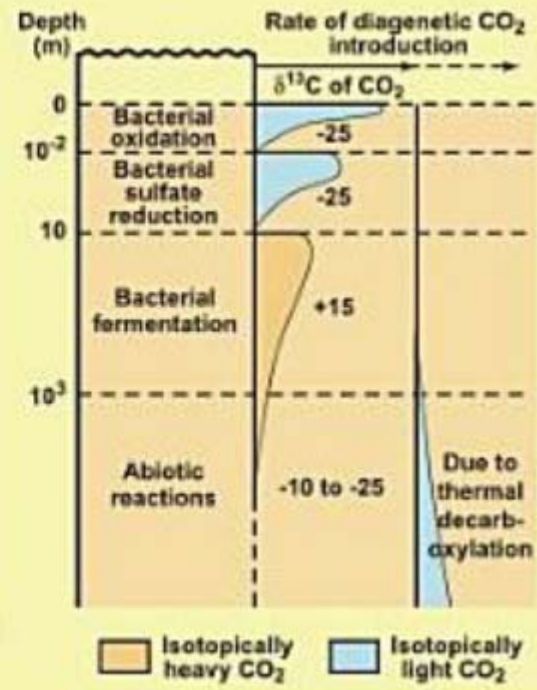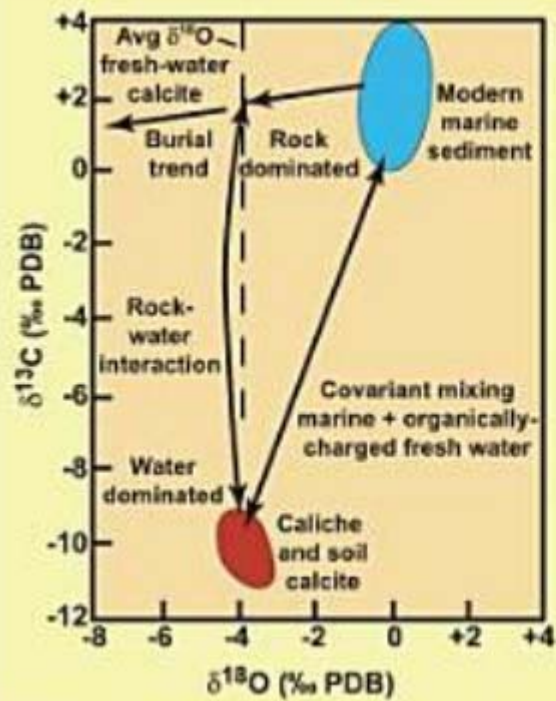
Fig. 1. Oxygen isotopic composition of atmospheric water vapor and precipitation from the tropical Atlantic Ocean across the Amazon Basin to Quelccaya. The ^{18}O depletion accompanying net water vapor loss from the air is calculated in three steps using a Rayleigh condensation equation, while 4) considers post-depositional isotope enrichment [Grootes et al., 1989]. Step 1). Water vapor depletion over the Amazon Basin varies from 0 % (dry season) to 85 % (wet season), resulting in a seasonal $\delta^{18}O$ change in precipitation of up to 18.4‰ ; Step 2), a 5.6 km increase in surface elevation from the Amazon Basin to Quelccaya results in a $\delta^{18}O$ decrease in precipitation of about 11‰; Step 3), strong convection in summer showers can increase the range of the seasonal $\delta^{18}O$ cycle by at least 5‰ (-10.5 to -33.7‰). Enrichment of $\delta^{18}O$ at the surface during the dry season may produce snow with $\delta^{18}O$ = -4.1‰. The observed range of $\delta^{18}O$ values in snow pits (-8.0 to -30.8‰) and its phase agree with the predicted range of -4.1 to -33.7‰.
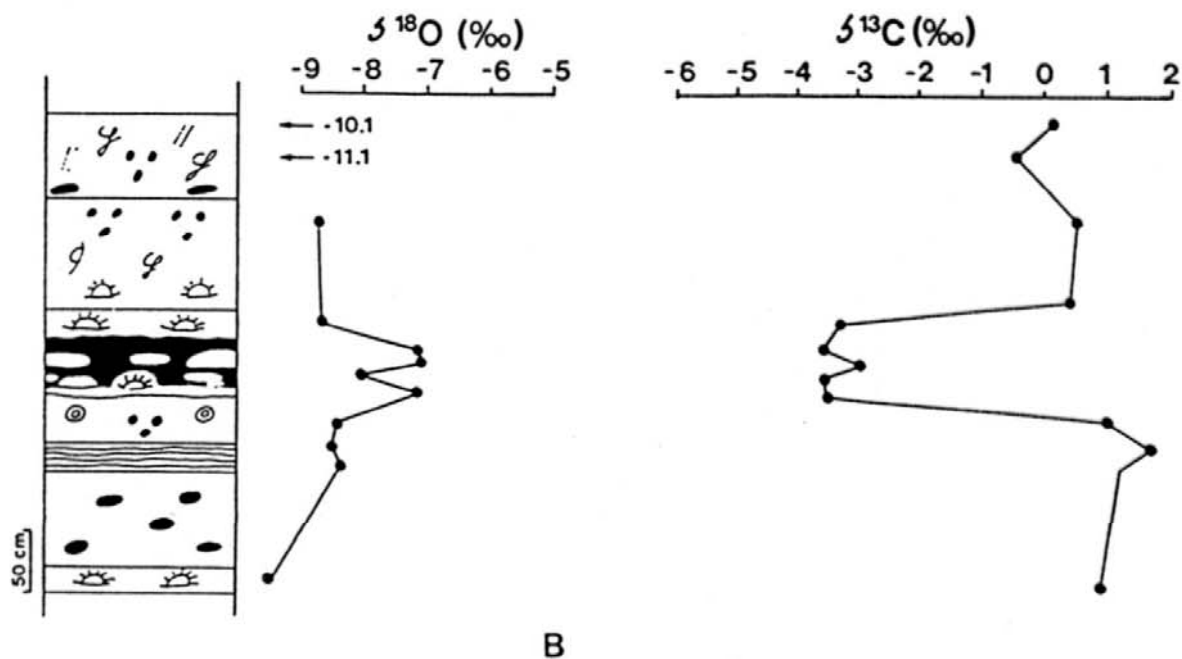
7

Up. Permian Wegener Halvo Fm., E. Greenland

8

Fig. 3. Carbon and oxygen isotopic composition of peritidal limestones and paleosols in the lower Viséan in the Flémalle-Haute (A) and Walhorn (B) quarries. The investigated paleosols occur at the top of the Terwagne Formation.
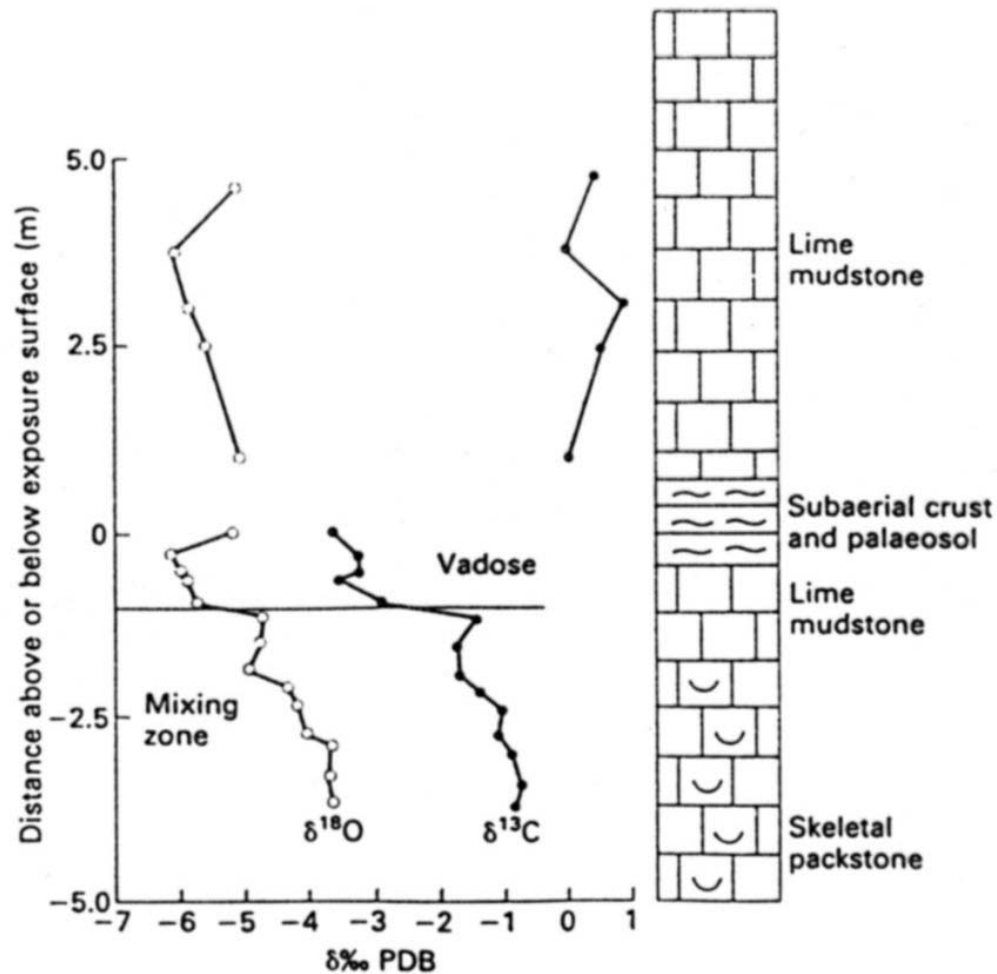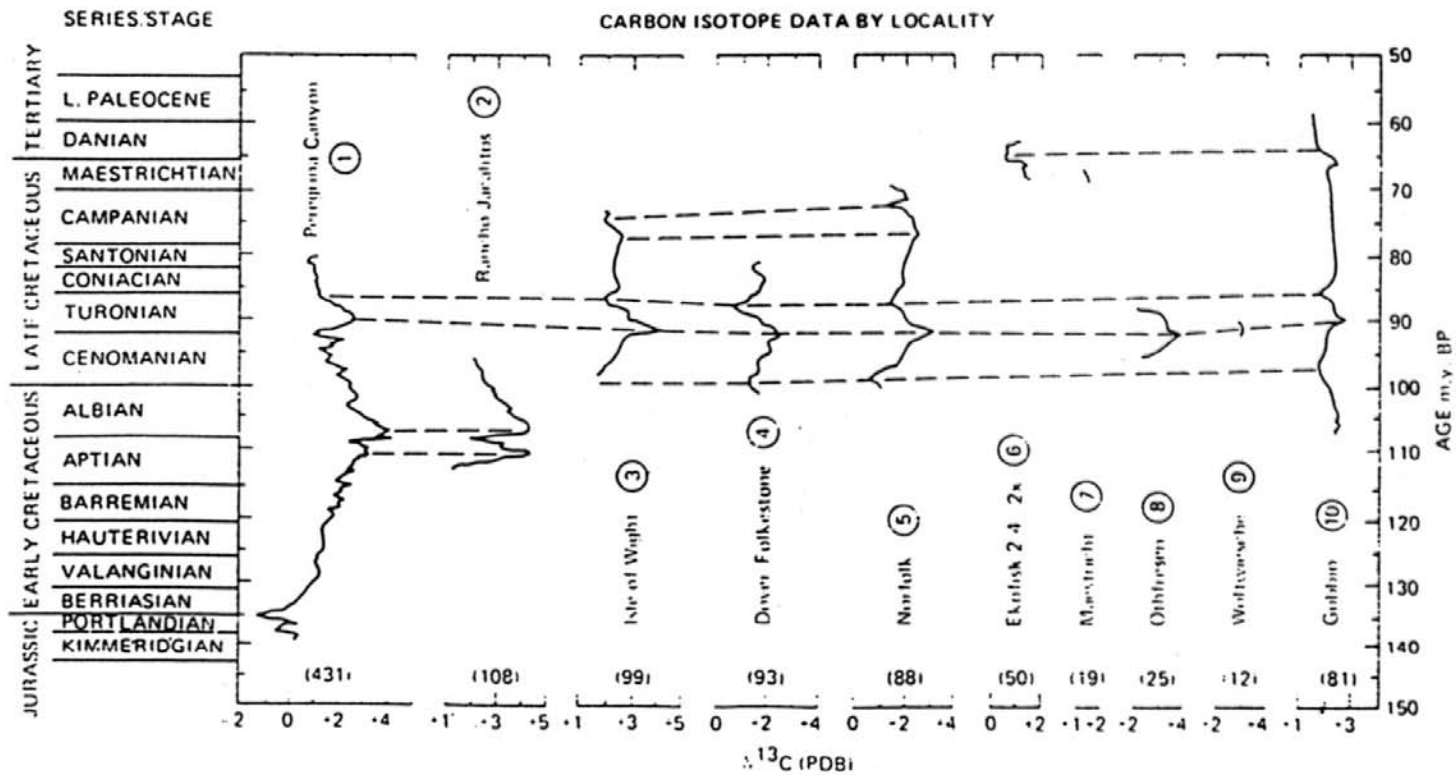
Fig. 9.31. Isotope profiles across a Mississippian emersion surface (Newman Limestone, Kentucky). Top five samples below exposure surface are depleted in ^{18}O and ^{13}C. Deeper samples show covariant increase in $\delta^{13}C$ and $\delta^{18}O$ thought to indicate diagenesis in marine-meteoric mixing zone. After Allan & Matthews (1982).

10

Chemostratigraphy

Figure 1-53. $\delta^{13}C$ stratigraphy of Cretaceous pelagic limestones from different global localities (after Scholle and Arthur, 1980). 1 and 2 - Mexico; 3-5-U.K.; 6 and 7 - North Sea and Netherlands; 8 and 9 - Germany; 10 Central Italy. Many new data have confirmed these patterns.
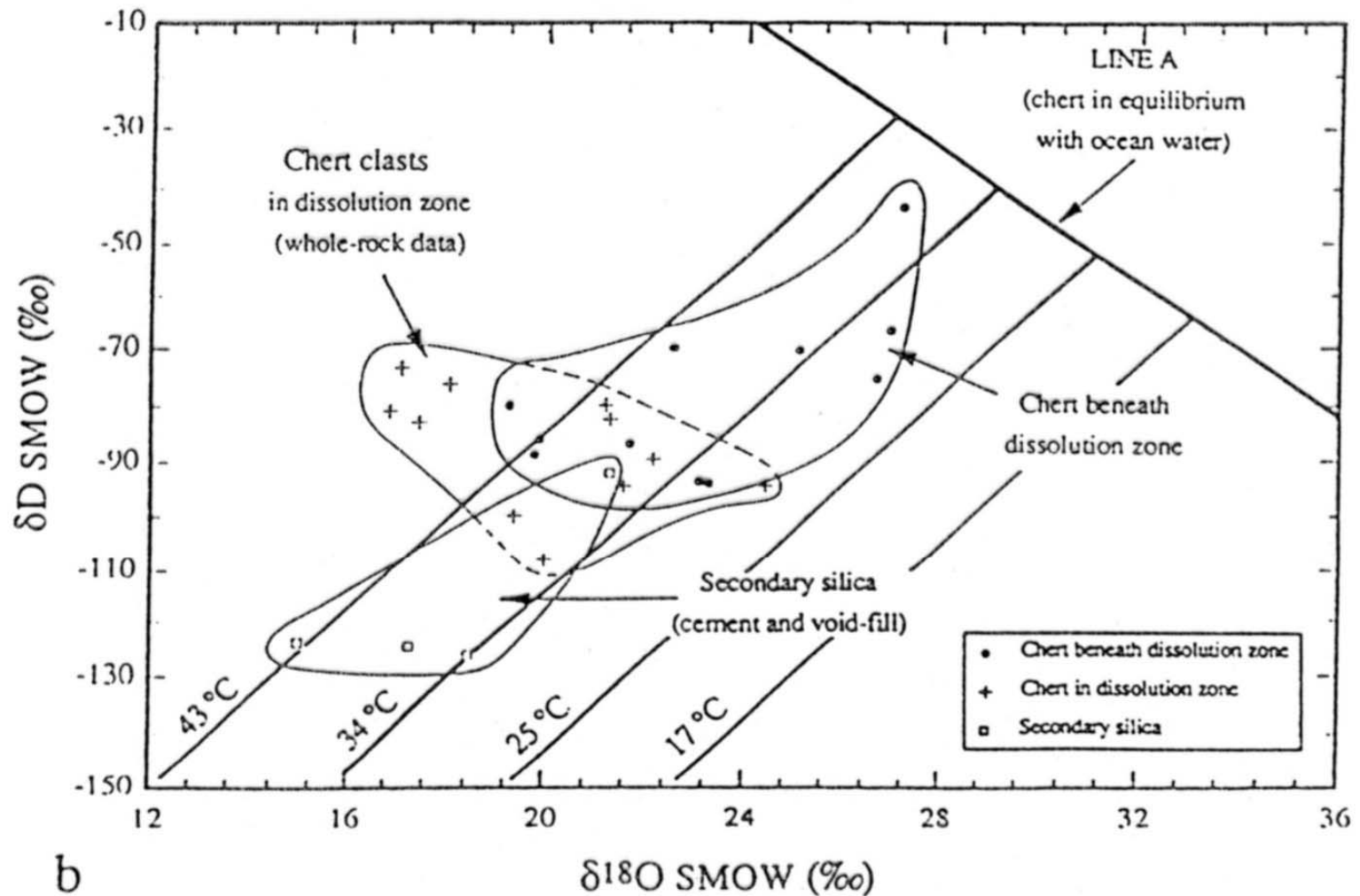
paleotemperatures

Figure 2. Isotopic composition of (a) Mescal and (b) Beck Spring cherts. Line A represents cherts in equilibrium with Standard Mean Ocean Water (SMOW), from Knauth and Epstein (1976). Temperatures of chert crystallization are from Knauth and Epstein (1976). Domains are strongly elongated in direction roughly parallel to meteoric water line. Early coastal chert δ values plot closest to line A; secondary silica values plot farthest away. Whole-rock samples include both early diagenetic and secondary chert.
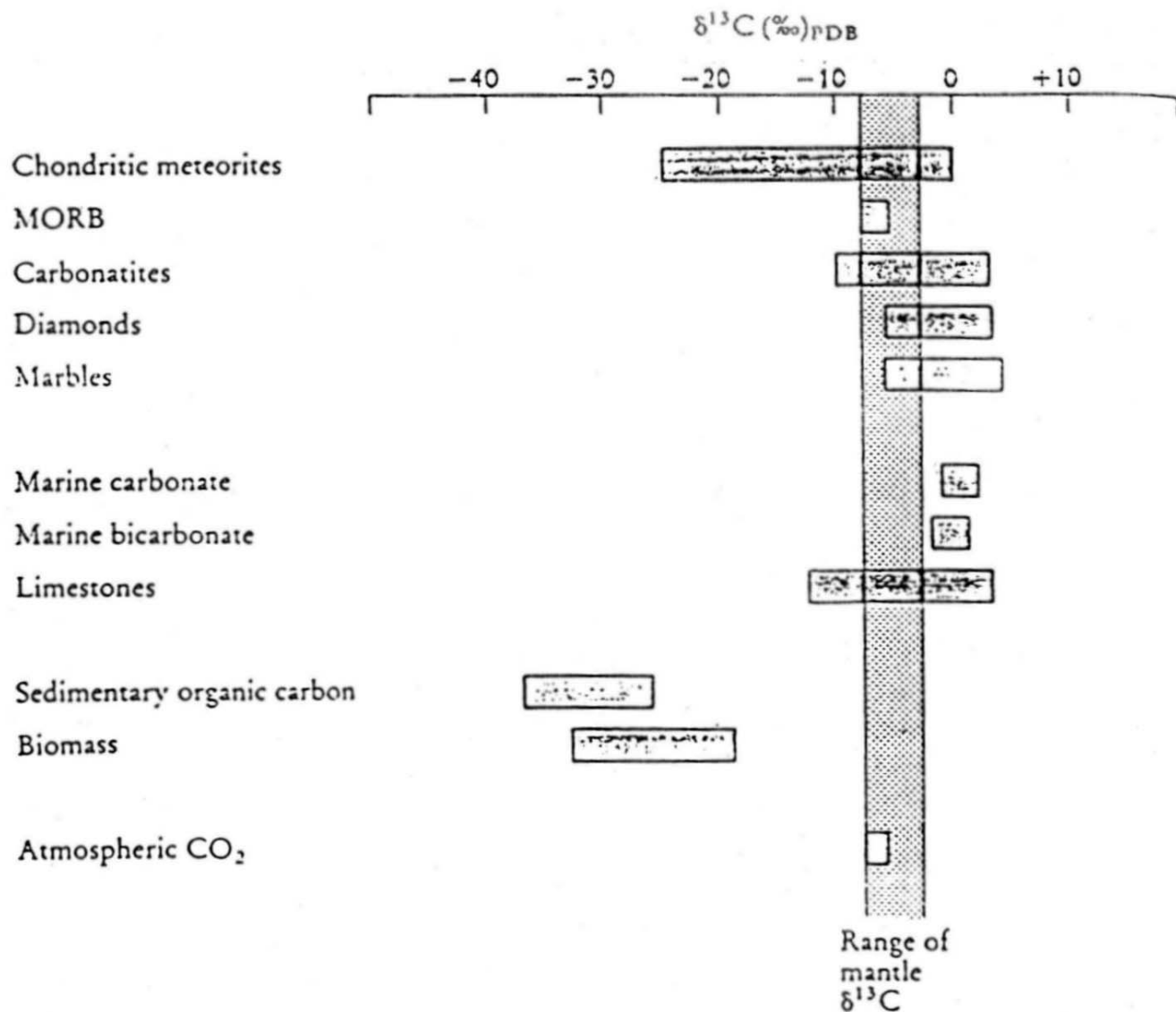
Carbon cycle

THE TERRESTRIAL CARBON SYSTEM, MAJOR RESERVOIRS AND FLUXES
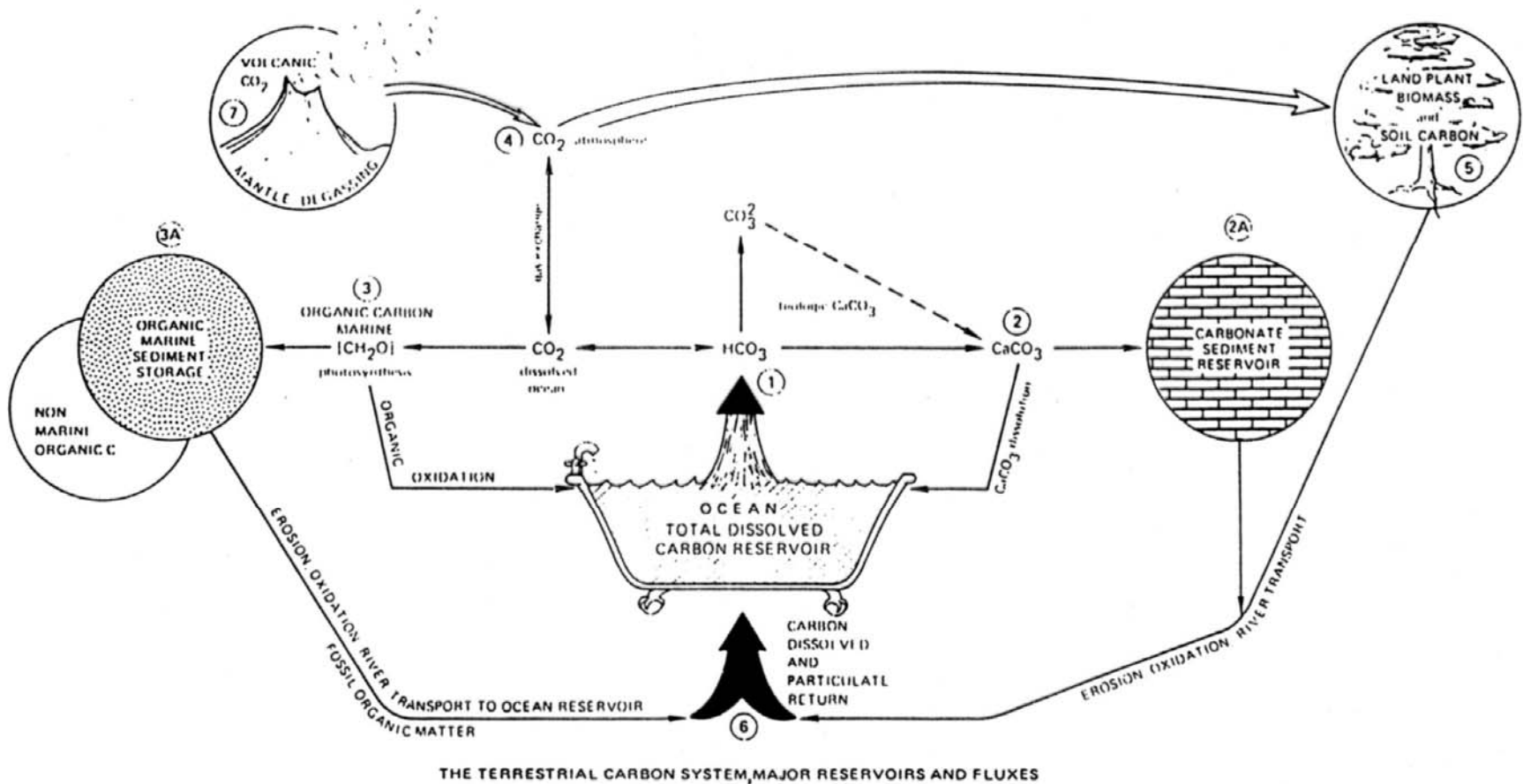
TDC – total dissolved carbon

Figure 1-30. Representation of major reservoirs and reservoir trans-
fers in the carbon cycle (after Scholle and Arthur, 1980). See
Table 1-4 for estimated masses, fluxes, and $\delta^{13}C$ values.

CO_2

CO_2
H_2O
O_2
CH_2O

H_2O O_2

SO_4^{2-} HS^-

CH_2O ⟶ CO_2

FeS_2

FeS_2
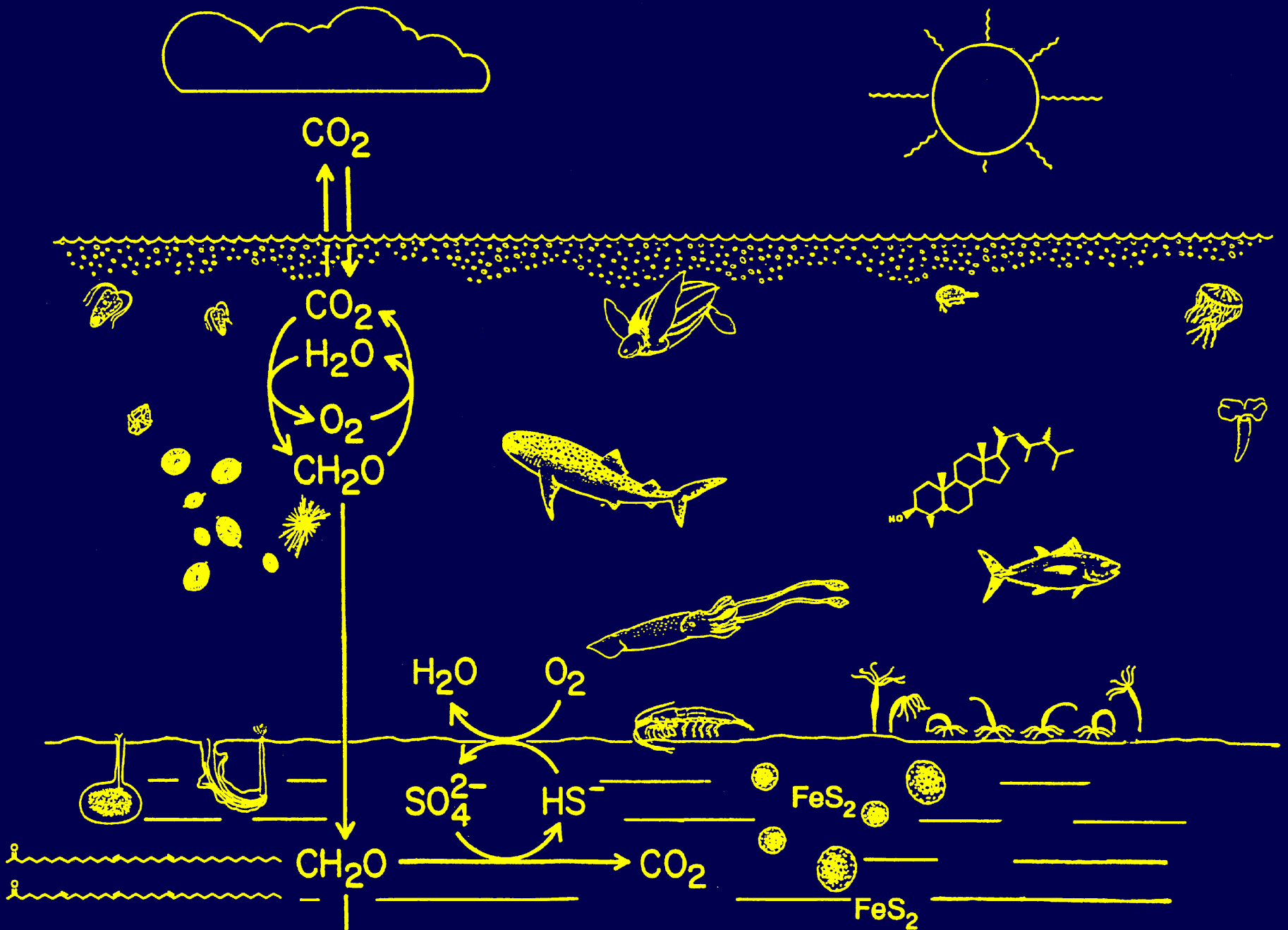
Natural $\delta^{13}C$ reservoirs. The ranges of $\delta^{13}C$ values in natural, carbon-bearing samples. Data from Kerridge (1985), Exley et al. (1986), Field and Fifarek (1986), Hoefs (1987) and Schidlowski (1987).
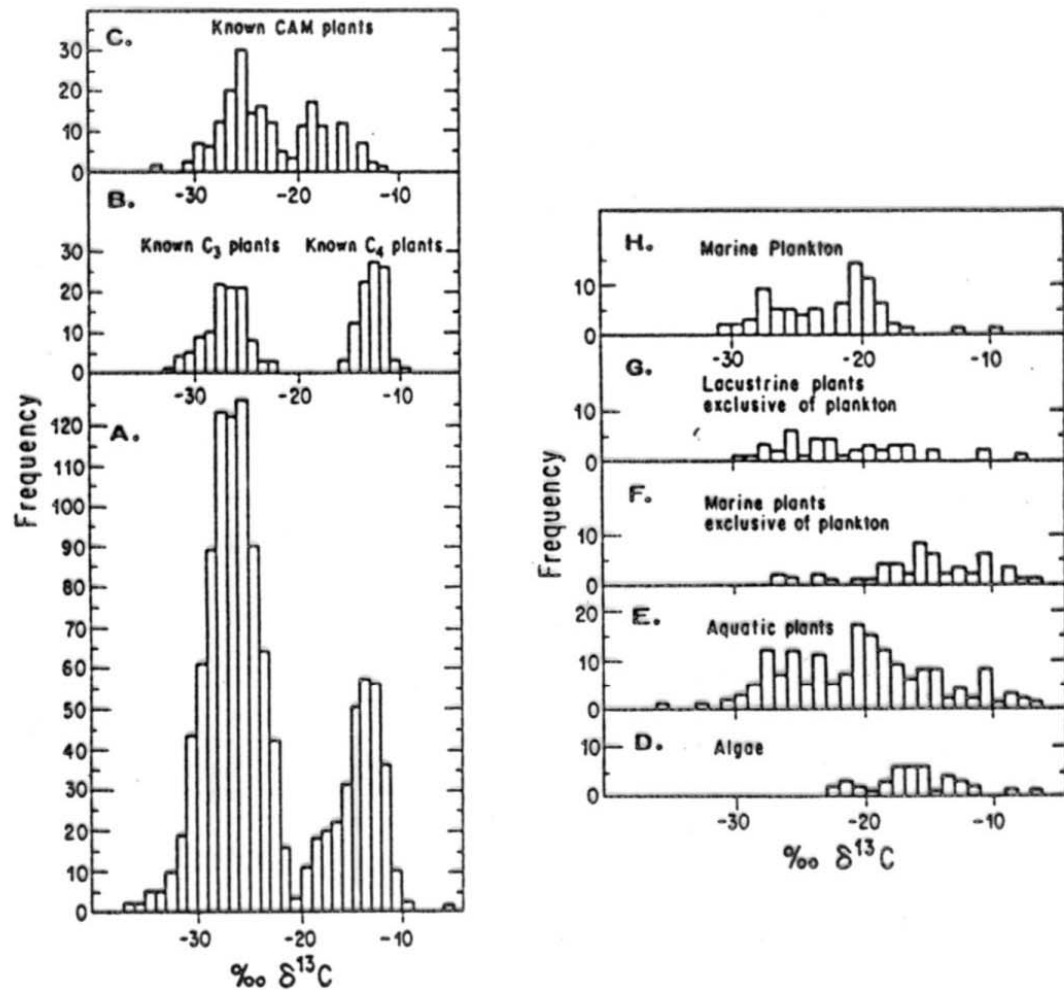
15

Fig. 9-3. Carbon isotopic composition of photosynthetically fixed carbon A. Terrestrial plants. B. Known C_3 and C_4 plants. C. Known CAM plants. D. Algae. E. Aquatic plants. F. Marine plants exclusive of plankton. G. Lacustrine plants exclusive of plankton. H. Marine plankton. Data from Bender (1968, 1971), Bender et al. (1973), Brown and Smith (1974), Craig (1953a), Deevey and Stuiver (1964), Degens et al. (1968b), Eadie (1972), Lerman et al. (1969), Lowdon and Dyck (1974), Oana and Deevey (1960), Osmond et al. (1975), Parker (1964), Sackett et al. (1965, 1974a), Smith and Brown (1973), Smith and Epstein (1970, 1971), Stahl (1968a), Troughton (1972), Wickman (1952), and Williams and Gordon (1970).
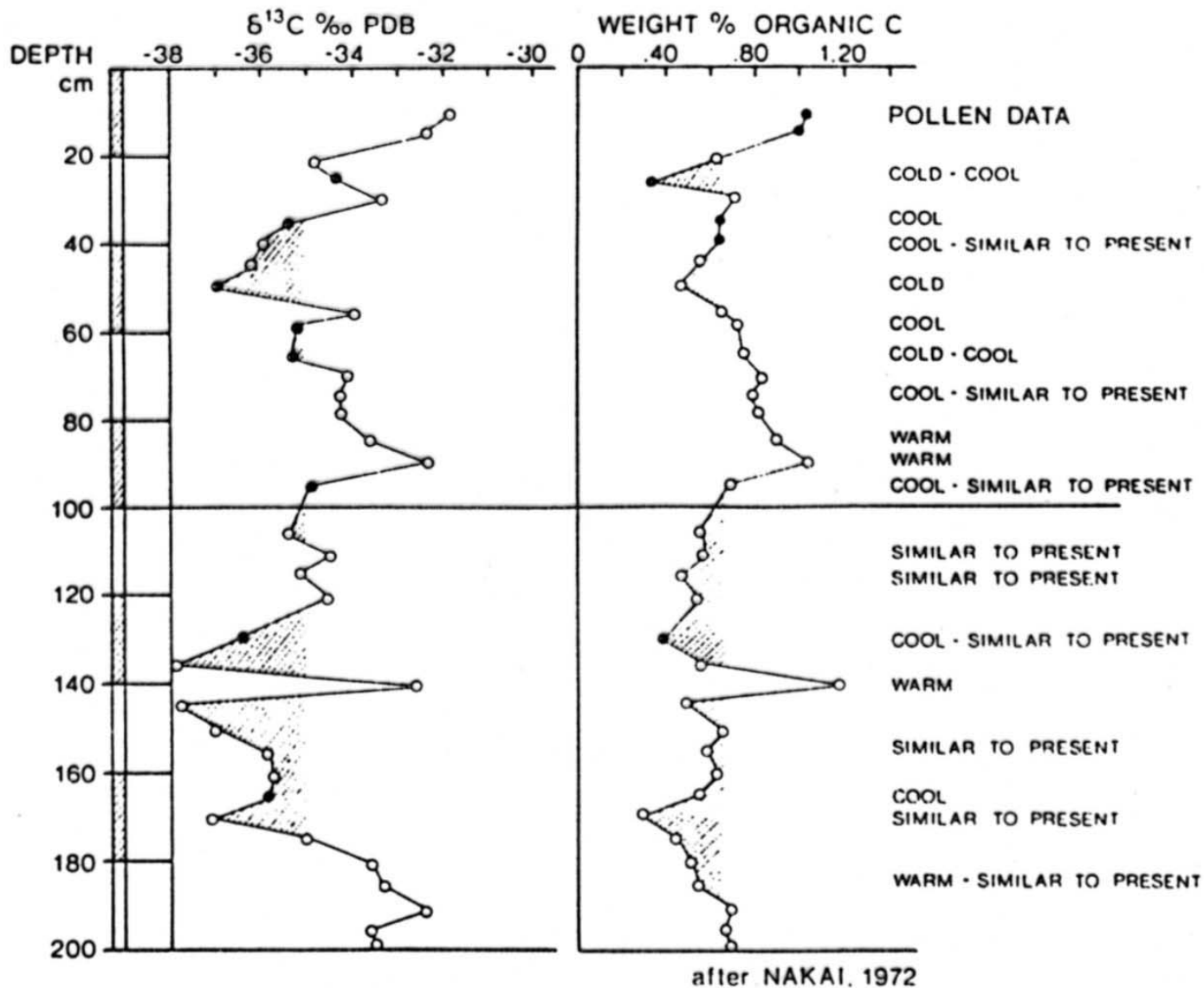
16

Fig. 12-3. A composition of ^{13}C data with organic carbon contents and pollen data from Lake Biwa (Japan) to document the agreement between paleoclimates and varying $\delta^{13}C$ values (after Nakai, 1972).

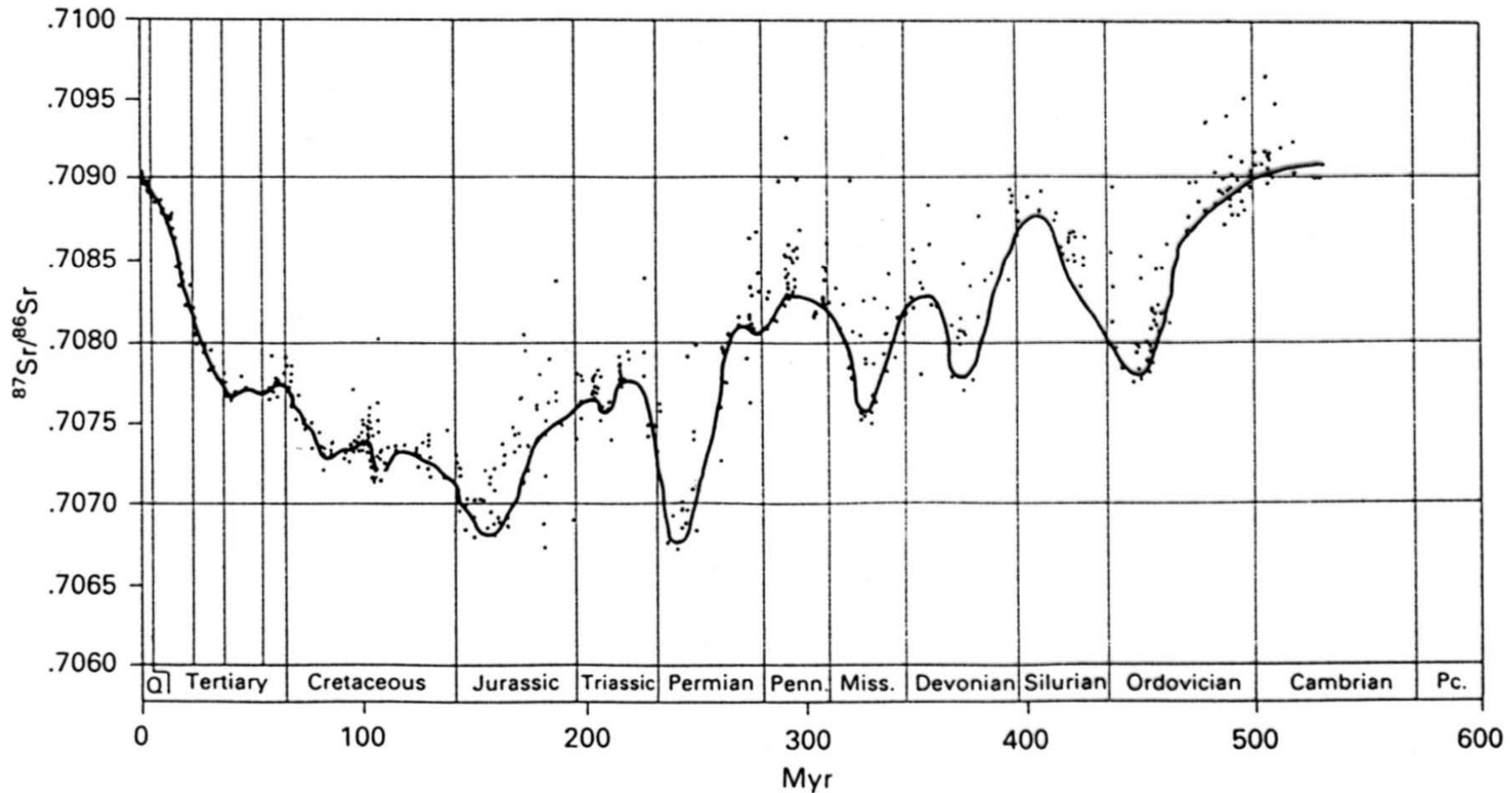# Strontium isotopes – stratigraphy, paleoenvironments

Fig. 9.34. Plot of Sr isotope variation with age of 744 samples of marine carbonates, evaporites and phosphorites (from Burke *et al.*, 1982). Data points scatter above the line because of diagenetic alteration and short-lived positive excursions (e.g. Cretaceous–Tertiary boundary, Hess, Bender & Schilling, 1986).
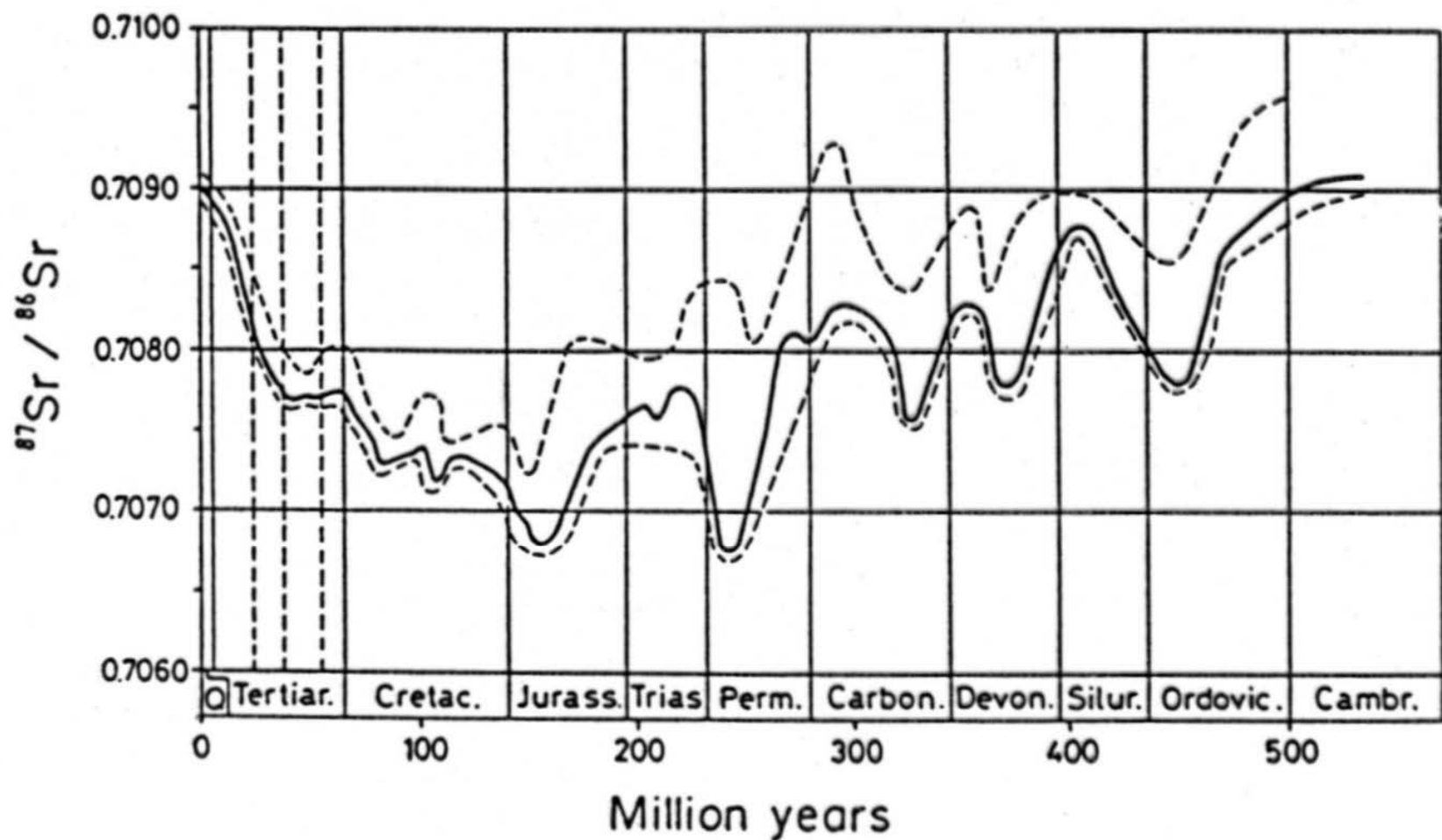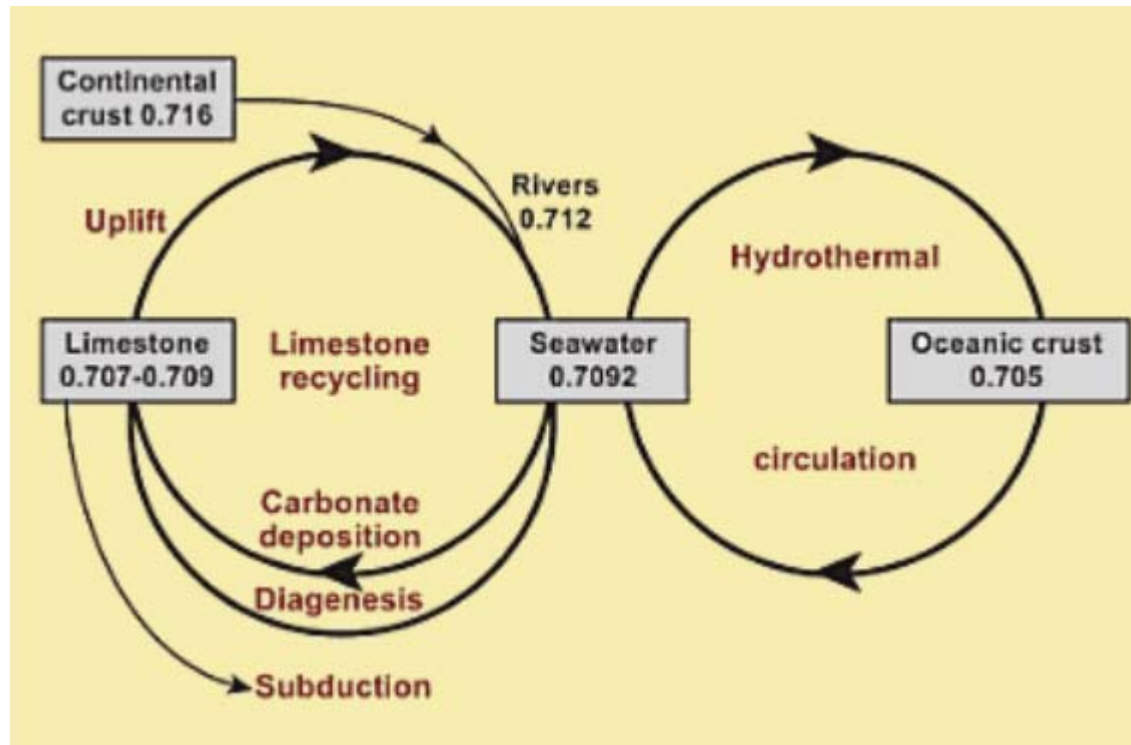
Fig. 5.2. Temporal variations of the Sr isotope ratio in seawater based on 786 isotopic analyses of marine carbonate rocks. The dashed lines show the extent of 95% of the data points. (Burke et al., 1982)
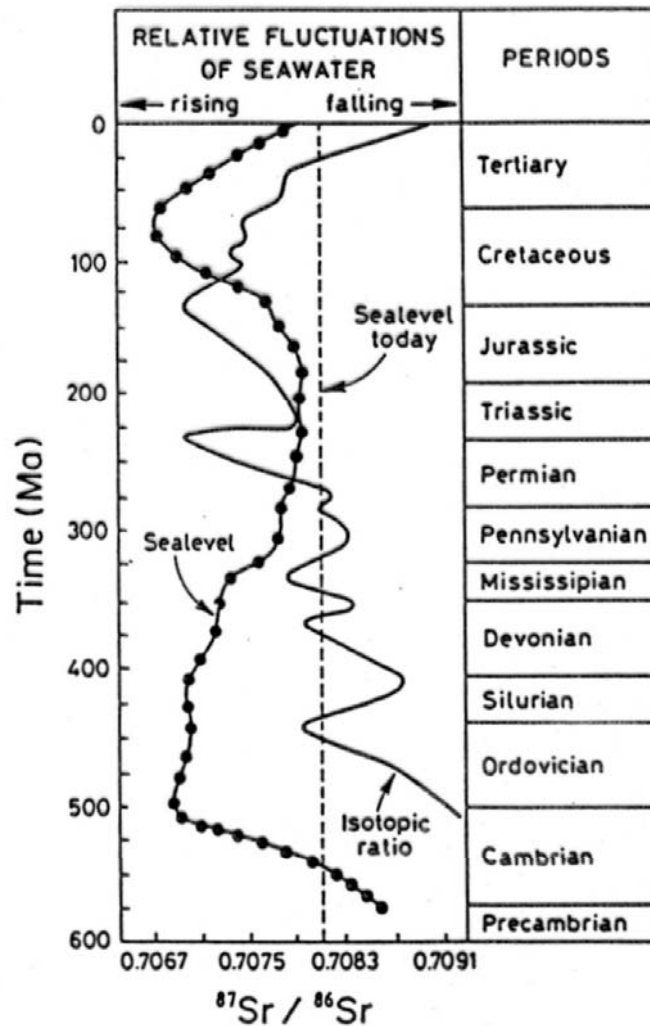
Strontium reservoirs and cycles

Fig. 5.15. Relationship between Sr isotopic variation in the oceans and sea level fluctuations through geologic time. Chauduri and Clauer (1986) were able to show that sealevel fluctuations and related hydrothermal seawater circulation are not always the majpr influences on the Sr isotopic composition of seawater. The authors postulate an additional source of Sr that supplies the oceans with relatively more radiogenic Sr groundwater.
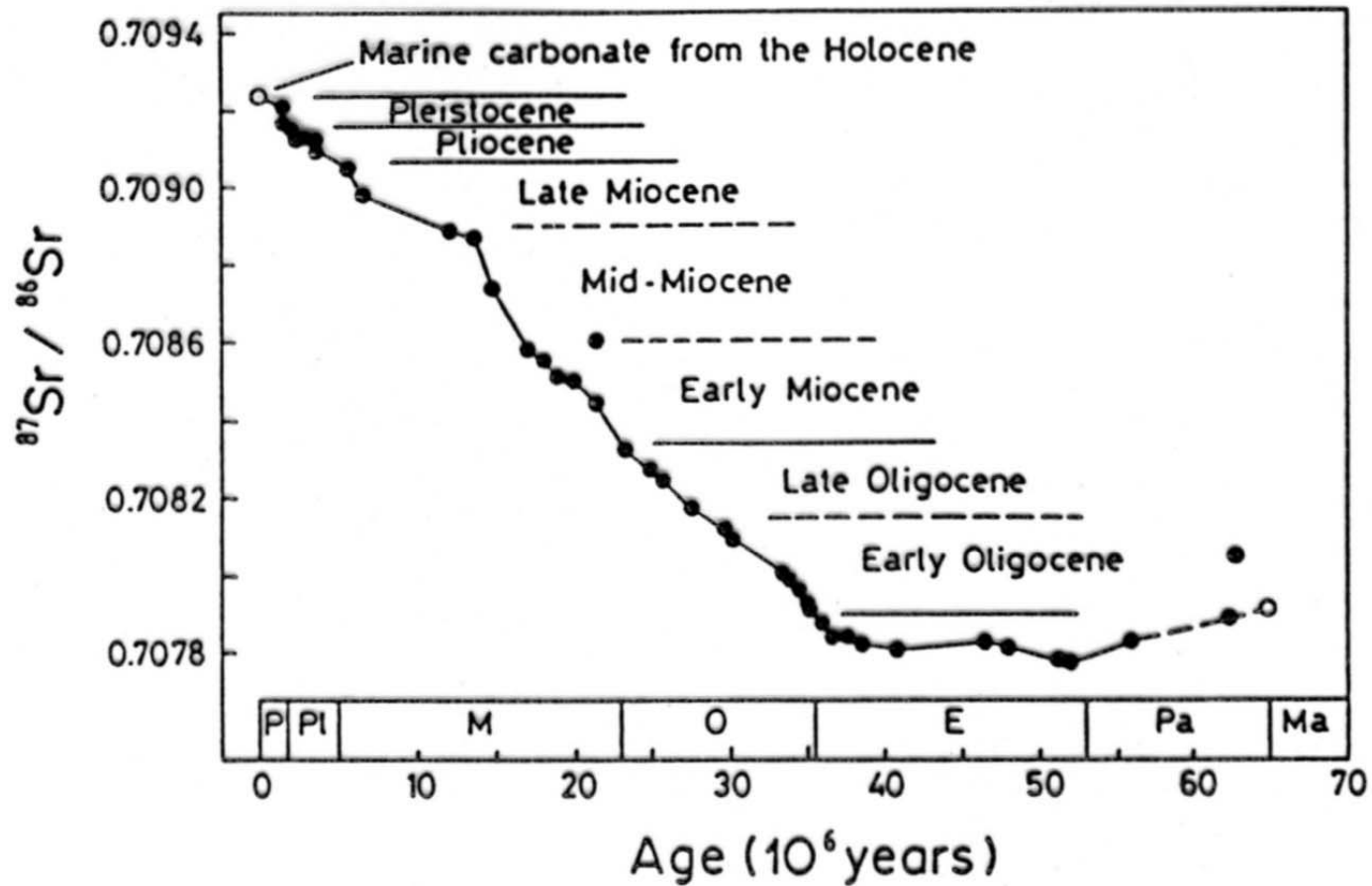
21

Fig. 5.3. The precise $^{87}Sr/^{86}Sr$ isotopic analyses of DePaolo and Ingram (1985) on stratigraphically well constrained marine carbonates allowed the reconstruction of a single clear trend in Tertiary seawater isotopic variation for the first time.
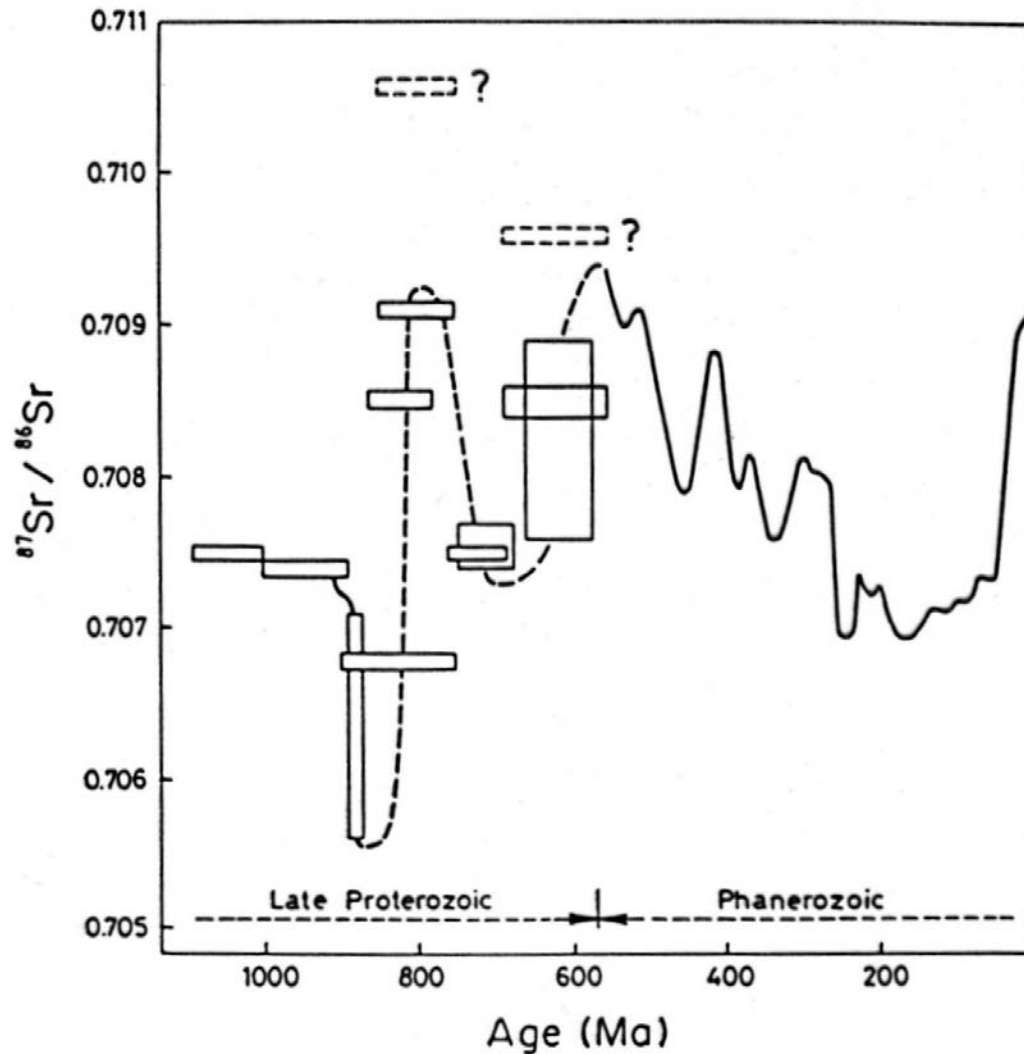
Fig. 5.8. The Sr isotopic composition of late Precambrian seawater. The lateral error bars represent stratigraphic uncertainties. The spread in the data is caused by reasons discussed in the text. (after Veizer and Compston 1974, 1976; Burke et al. 1982)

23

Cathode luminiscence (CL)

principles: excitation by electron beam, emission of radiance

Mn^{2+} luminiscence activator, Fe^{2+} luminiscence inhibitor in carbonates

study of carbonate and quartz cements, recrystallization processes → cement stratigraphy, fluid composition and migration history

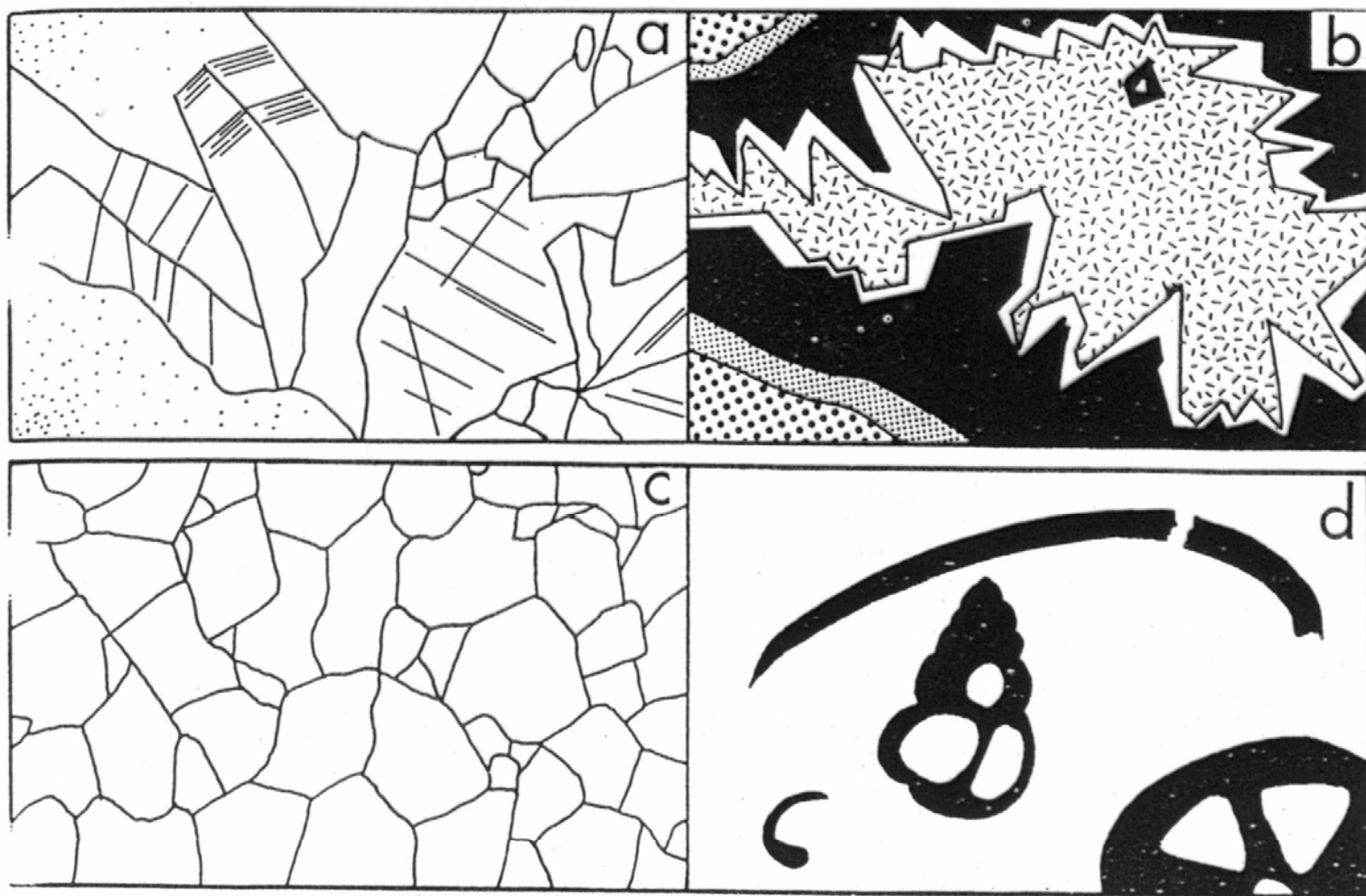provenance of clastic material – quartz typology

Fig. 6.3. Drawings made from photographs of CL in limestones from the Dinantian (Lower Carboniferous) of Ireland. (a) Coarse sparry calcite mass seen in transmitted light. (b) Same view but with cathodoluminescence, showing a void developed in micrite (coarse stipple), with a cement sequence of radial fibrous spar (light stipple), non-luminescent ferroan calcite (black) and brightly luminescent outer zone (white). The void fill is completed by dolomite (hashures). (c) Medium-grained blocky spar mosaic seen under transmitted light is revealed under cathodoluminescence (d) as a neomorphosed, brightly luminescent biomicrite with gastropods, bivalves and foraminifera which are weakly luminescent.
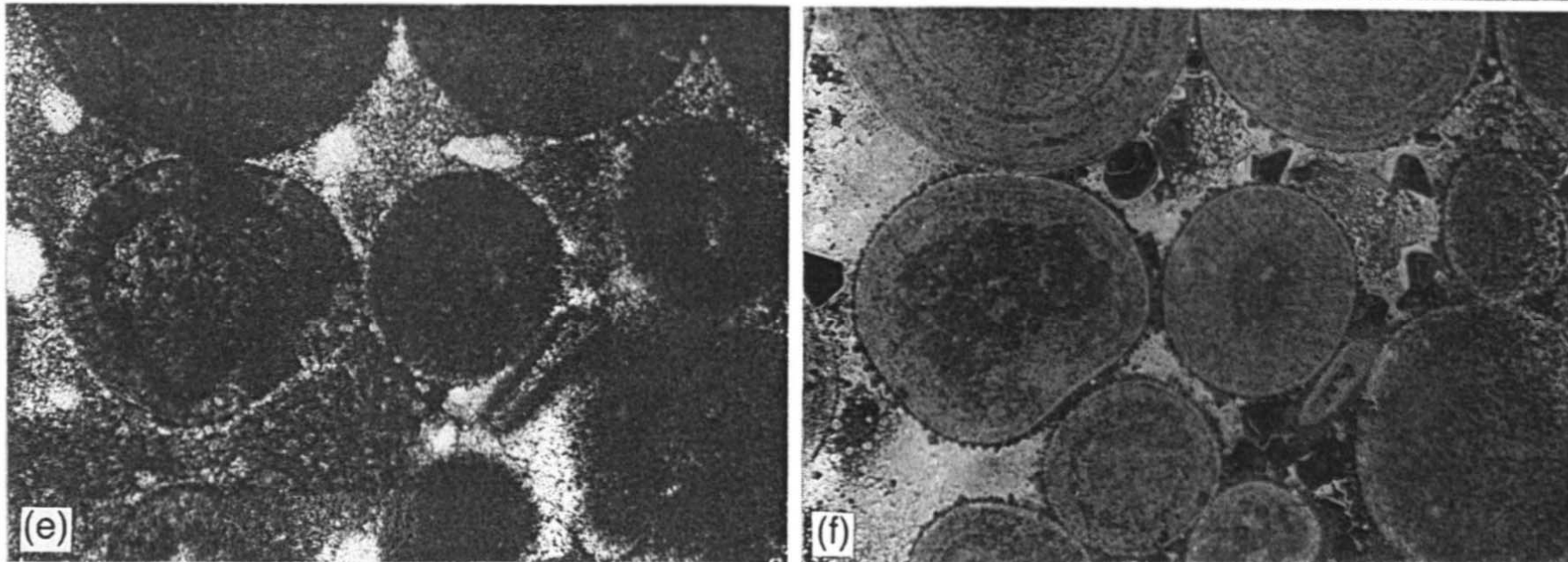
25
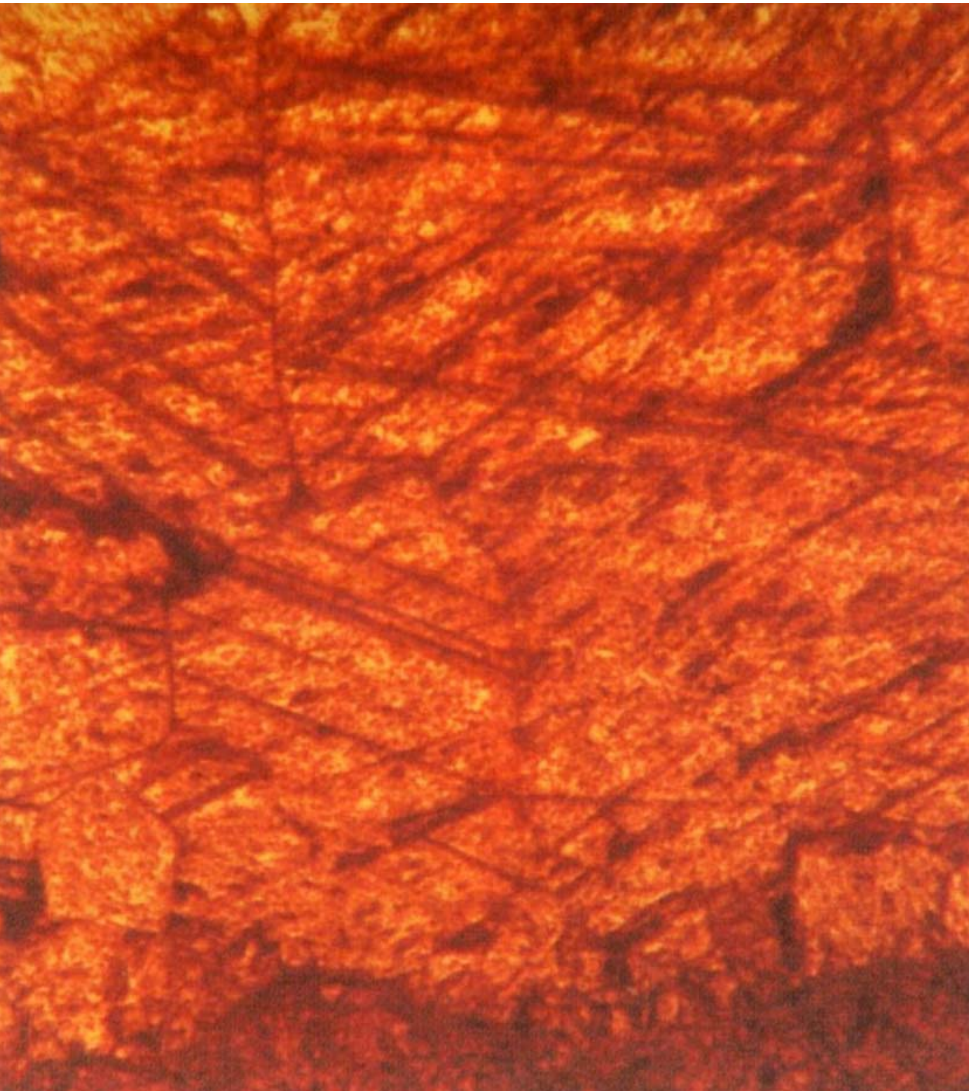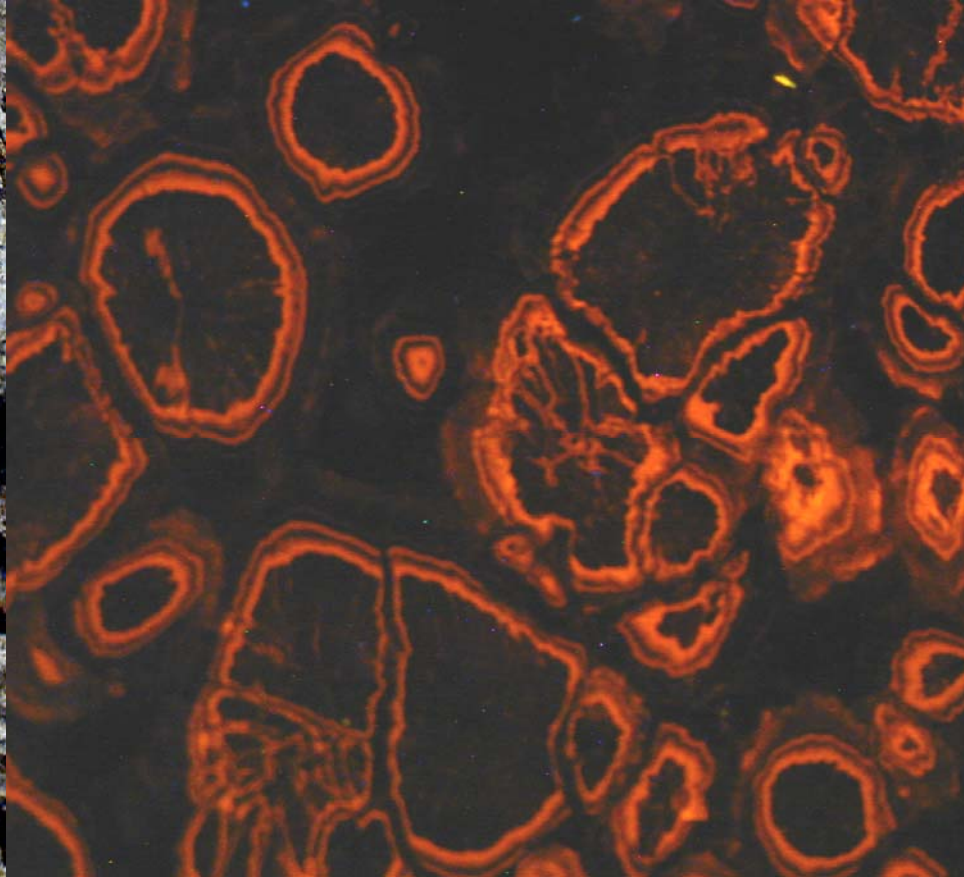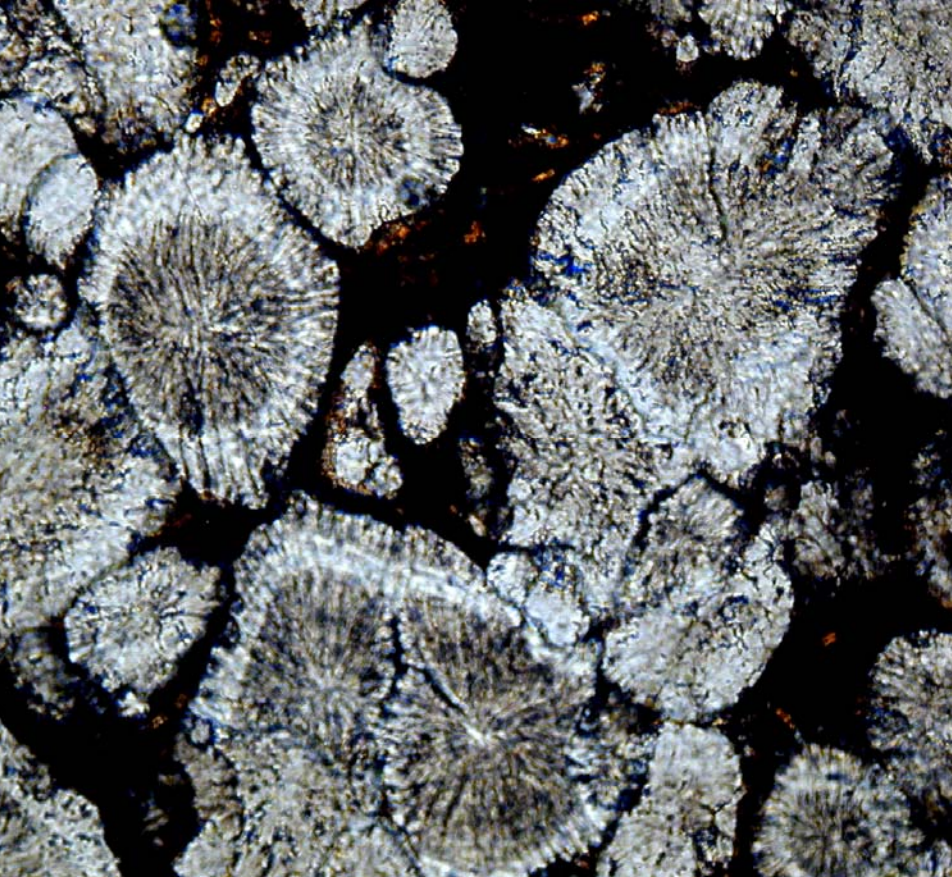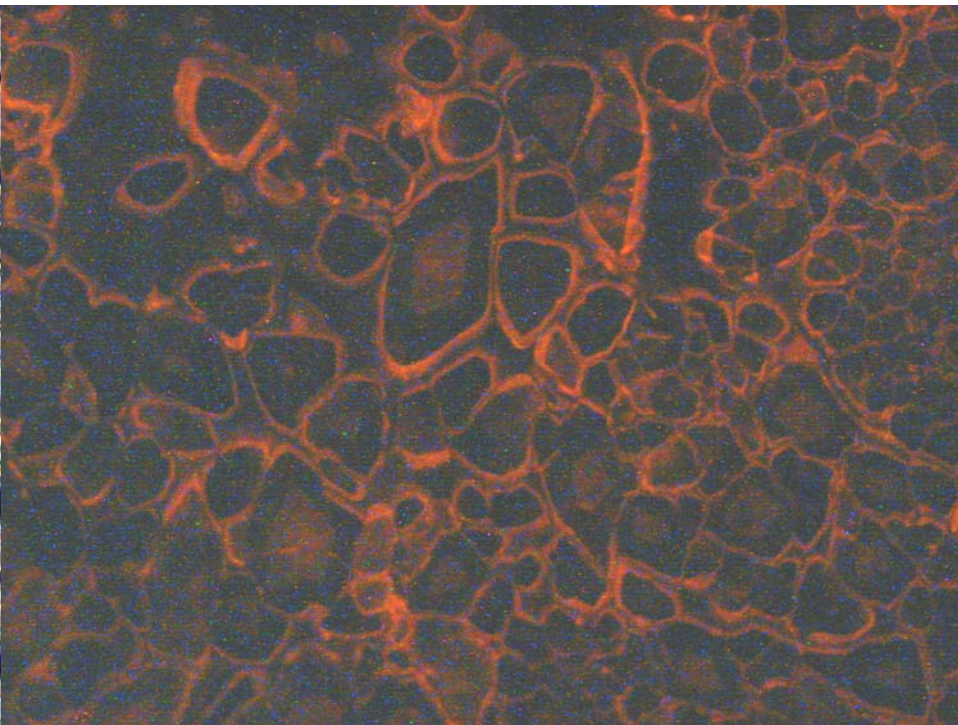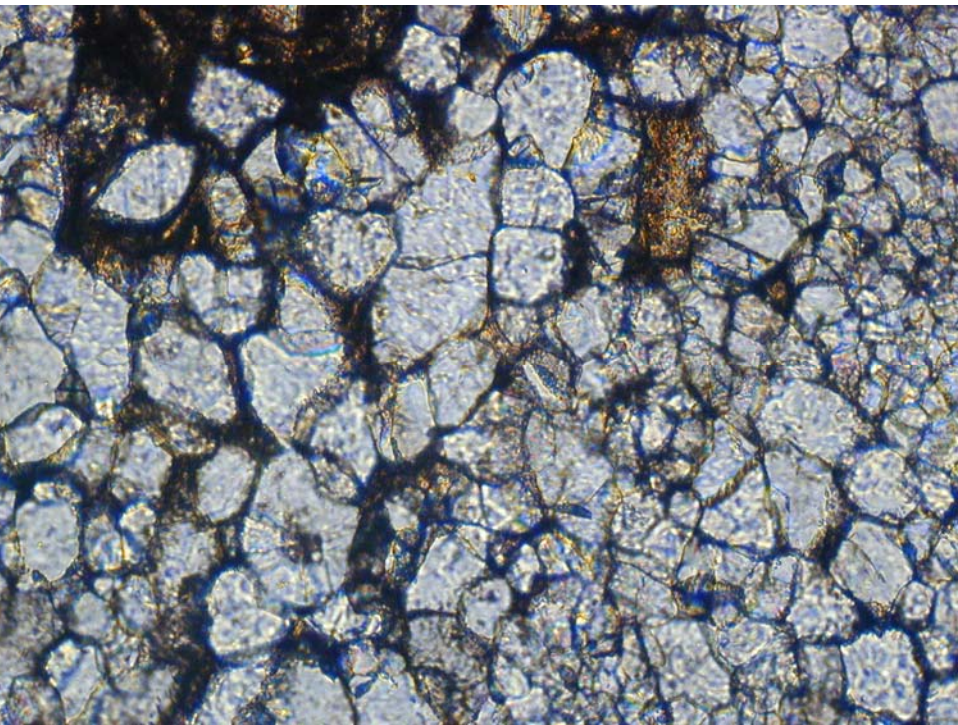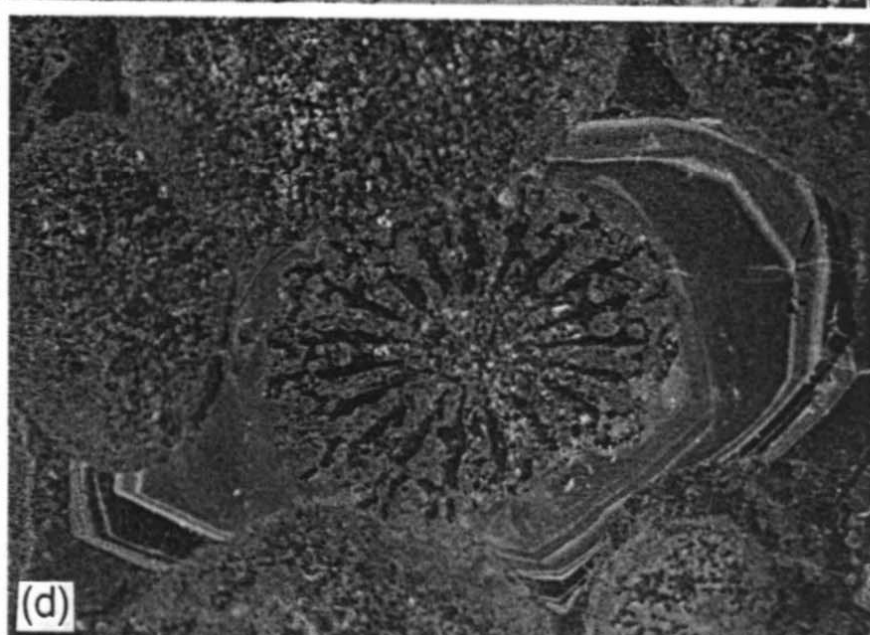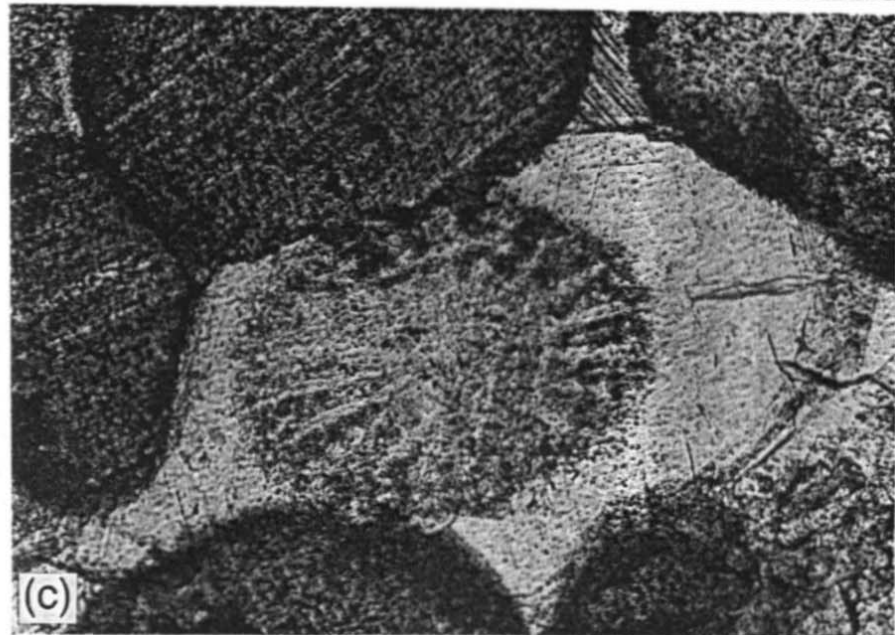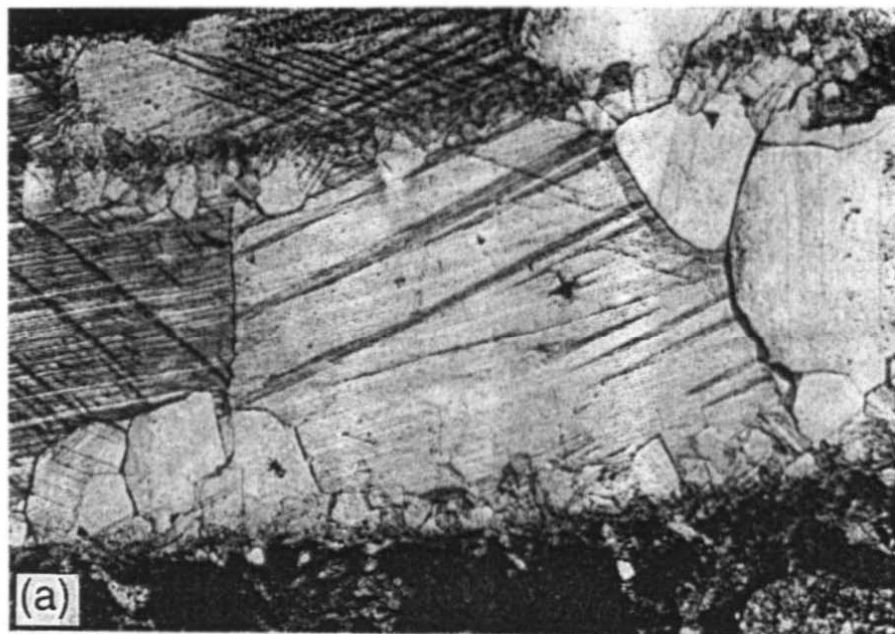
Fig. 6.4. Paired photomicrographs of limestone thin sections, with transmitted light view to the left and cathodoluminescence view to the right. All from the Dinantian (Lower Carboniferous) of South Wales. (a), (b) Pwll-y-Cwm Oolite. Calcite cement fill of bivalve mould, showing details of crystal growth by fine luminescent and non-luminescent growth bands. (c), (d) Blaen Onneu Oolite. Syntaxial calcite overgrowth on an echinoid spine, showing preferential nucleation on the crystallographically suitable substrate. CL reveals detail of the internal structure of the recrystallized spine. Changes in CL intensity in the overgrowth cement are due to varying concentrations of Fe^{2+} quencher. (e), (f) Gilwern Oolite. Details of the internal structure of ooids is better revealed by CL. Thin, non-luminescent calcite cement fringes occur on the ooids, followed by brightly-luminescent microspar associated with calcrete formed during subaerial exposure. Photographs by courtesy of Dr M. Raven.

30
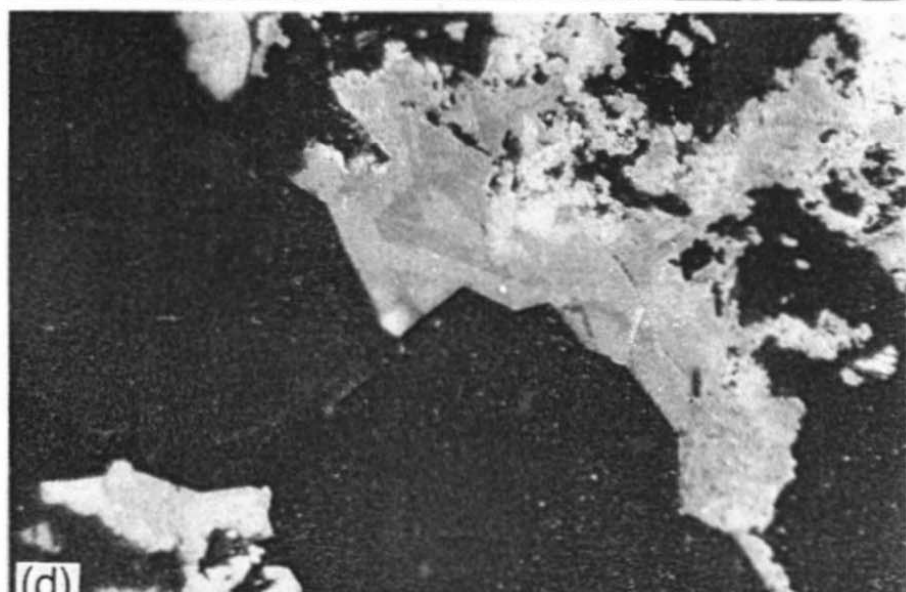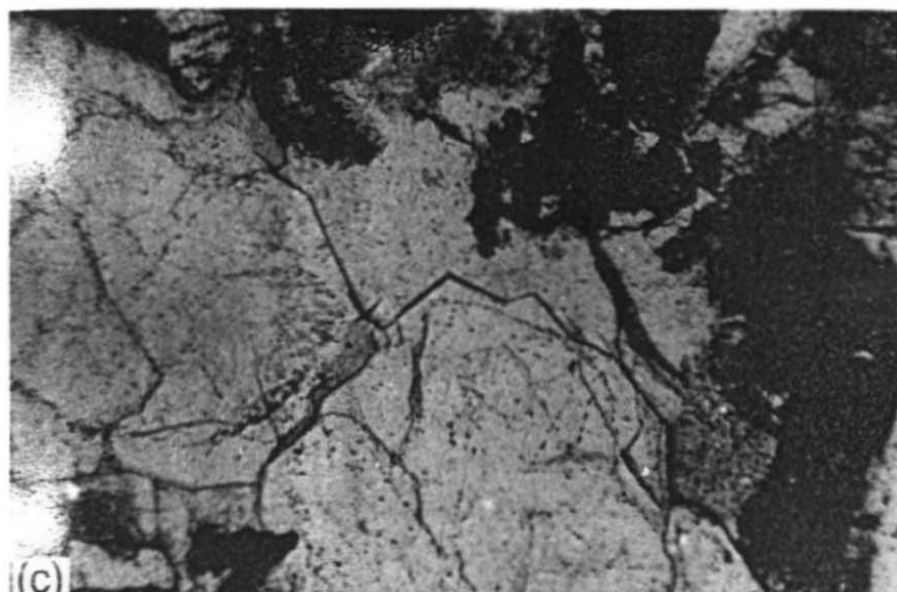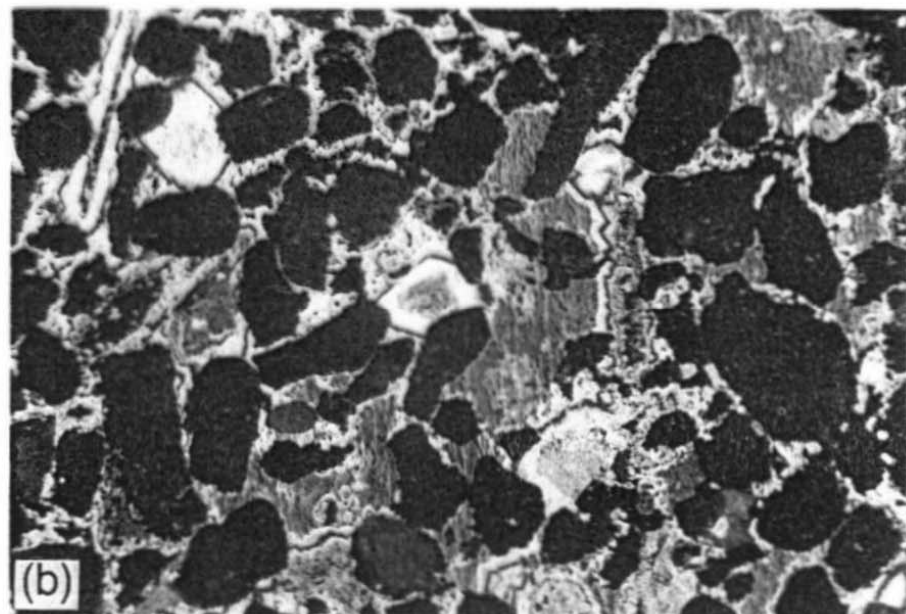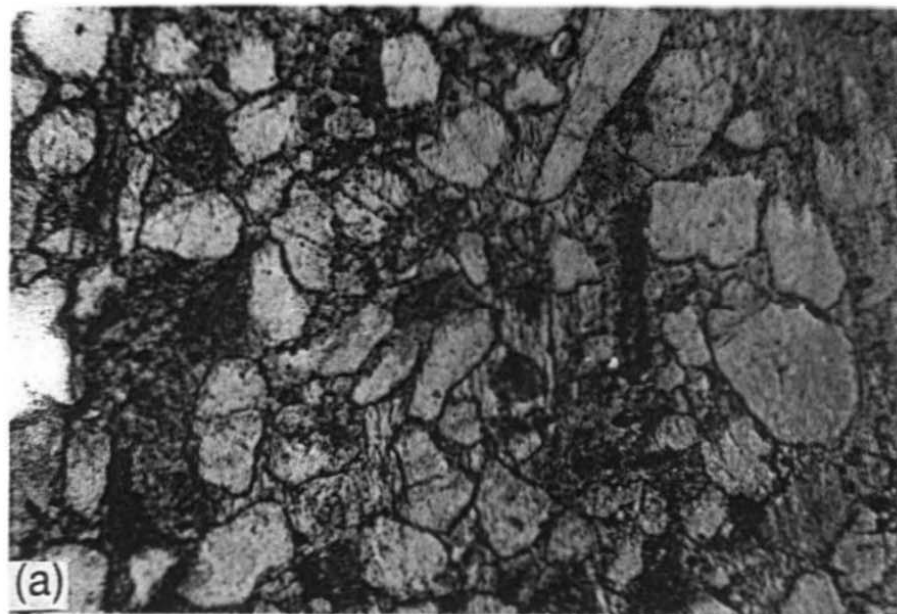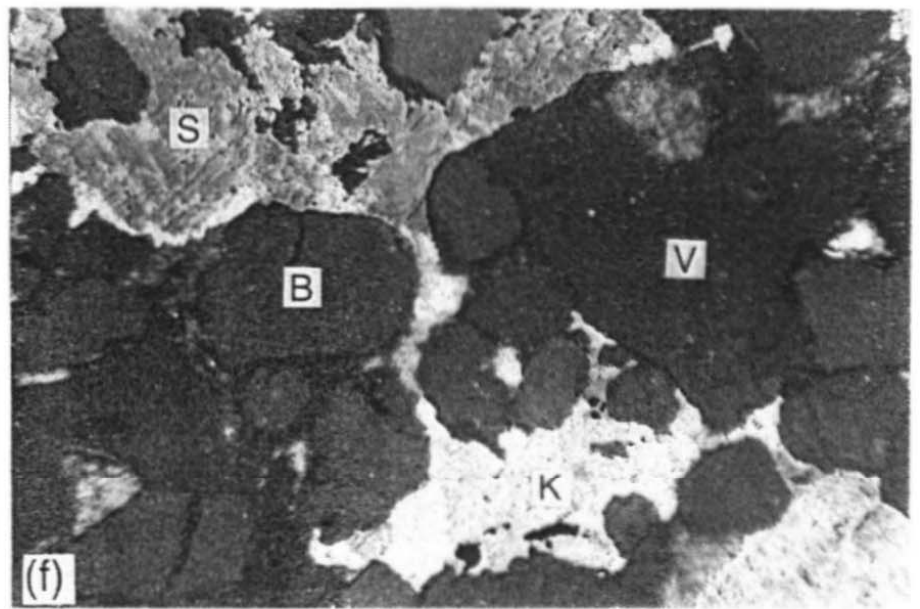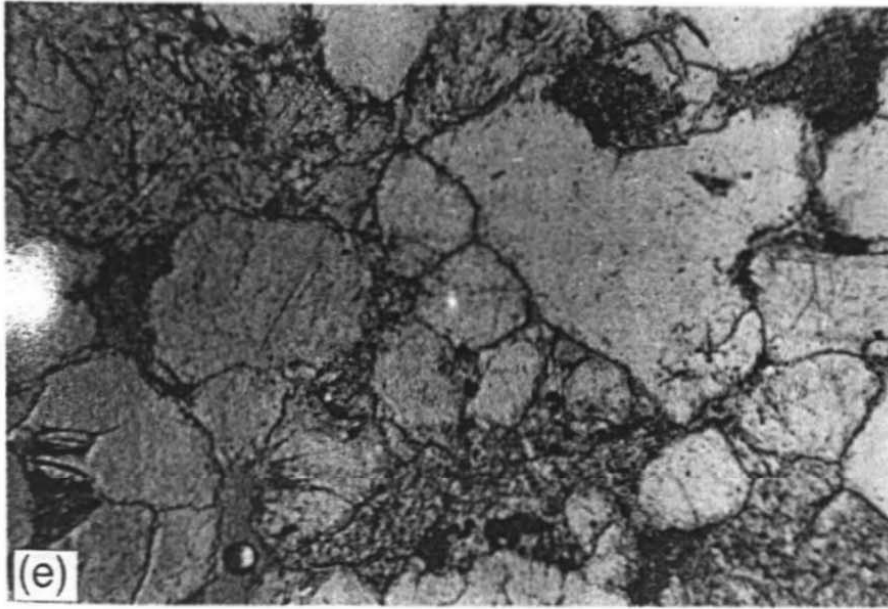
6.5. Paired photomicrographs of sandstones from North Sea cores, transmitted light view to the left and CL view to the right. (a), (b) Medium-grained sandstone with a carbonate cement is seen under CL to have a fairly high fossil content, mainly echinoderms: crinoid fragments and an echinoid spine (top left) provide substrates for large, zoned overgrowths which have occluded the primary porosity. (c), (d) Coarse sandstone with non-luminescent authigenic quartz overgrowths on violet-luminescing quartz grains. A subsequent zoned calcite cement is being dissolved by kaolinite (white on picture, royal blue CL). (e), (f) Violet luminescing (V) and brown (B) quartz grains showing a mixture of metamorphic and igneous sources. A sparry calcite cement (S) is suffering dissolution by brightly-luminescing kaolinite (K).

Reading:

J.Miller (1988): Cathodoluminiscence microscopy. In: M.Tucker ed.: Techniques in sedimnetology, Blackwell.

D.J.Marshall (1988): Cathodoluminiscence of geological materials. Unwin Hyman, Boston.

P.Stille a G.Shields (1997): Radiogenic isotope geochemistry of sedimentary and aquatic systems. Lecture notes in Earth sciences 68, Springer.

J.Hladíková (1988): Základy geochemie stabilních izotopů lehkých prvků. skripta PřF UJEP, Brno.

G.Faure (1986): Principles of isotope geology. John Wiley&sons.

P.Fritz a J.Ch.Fontes eds (1980): Handbook of environmental isotope geology. Elsevier.

P.K.Swart et al. eds. (1993): Climate change in continental isotopic records. Geophysical monograph 78, AGU.

L.Pratt et al. : Geochemistry of organic matter in sediments and sedimentary rocks. SEPM short course 27.

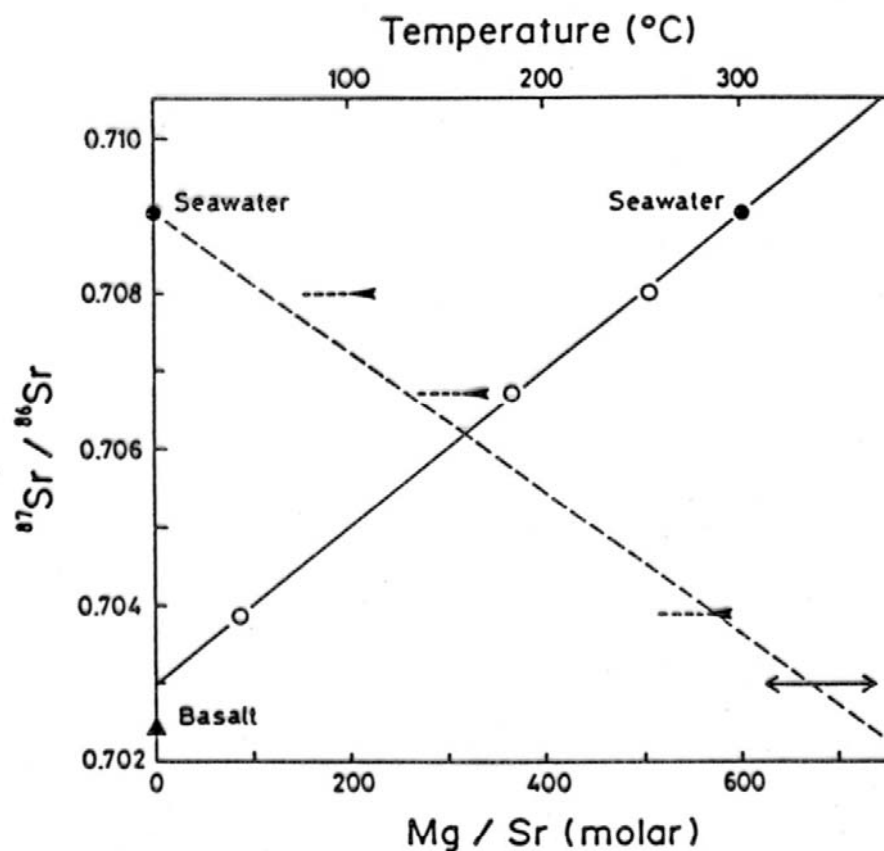J.Parnell et al. (1993): Bitumens in ore deposits. Springer.

Fig. 5.1. The seawater $^{87}Sr/^{86}Sr$ and Mg/Sr ratios near the 'Galapagos spreading center' (Pacific) show clearly that local seawater has been influenced by mantle Sr. If all the Mg in this mixing system derives from seawater it can be assumed that the hydrothermal fluid system uncontaminated with seawater must show a similar $^{87}Sr/^{86}Sr$ ratio to basalt, i.e. 0.703. A simple correlation between water chemistry and temperature (arrows) allows the temperature of the hydrothermal fluid phase to be determined at 340 °C. (Albarède et al. 1981)
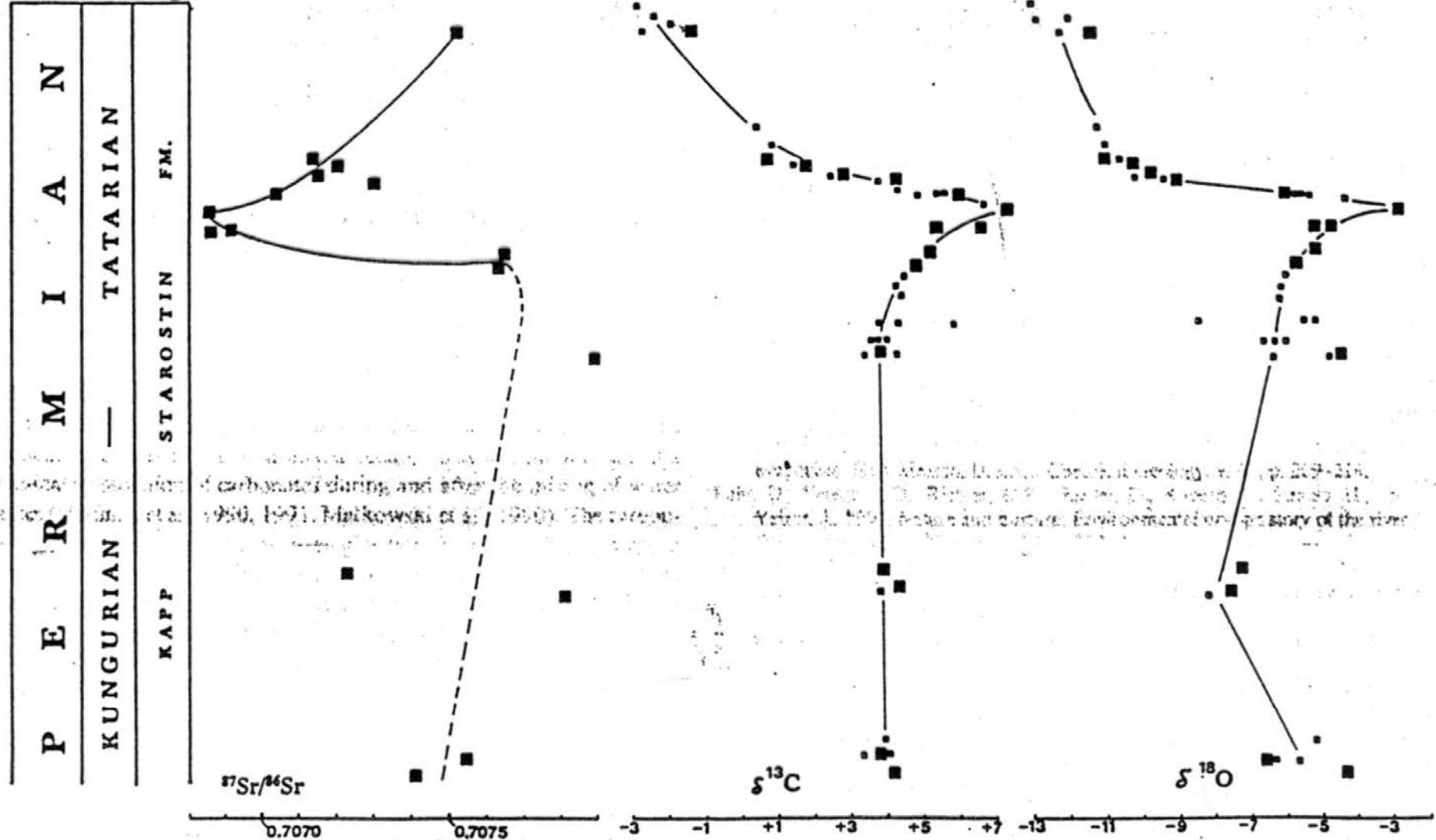
35

Figure 1. Strontium, carbon, and oxygen isotope curves for Kapp Starostin Formation, West Spitsbergen. Large black squares denote brachiopod samples analyzed for all three isotopic ratios; small squares indicate those analyzed for carbon and oxygen isotopes only. Dashed line in lower part of strontium isotope curve indicates that sampling was too sparse to draw firm conclusions about course of events. For sample location and geologic setting, see Małkowski et al. (1988, 1991).
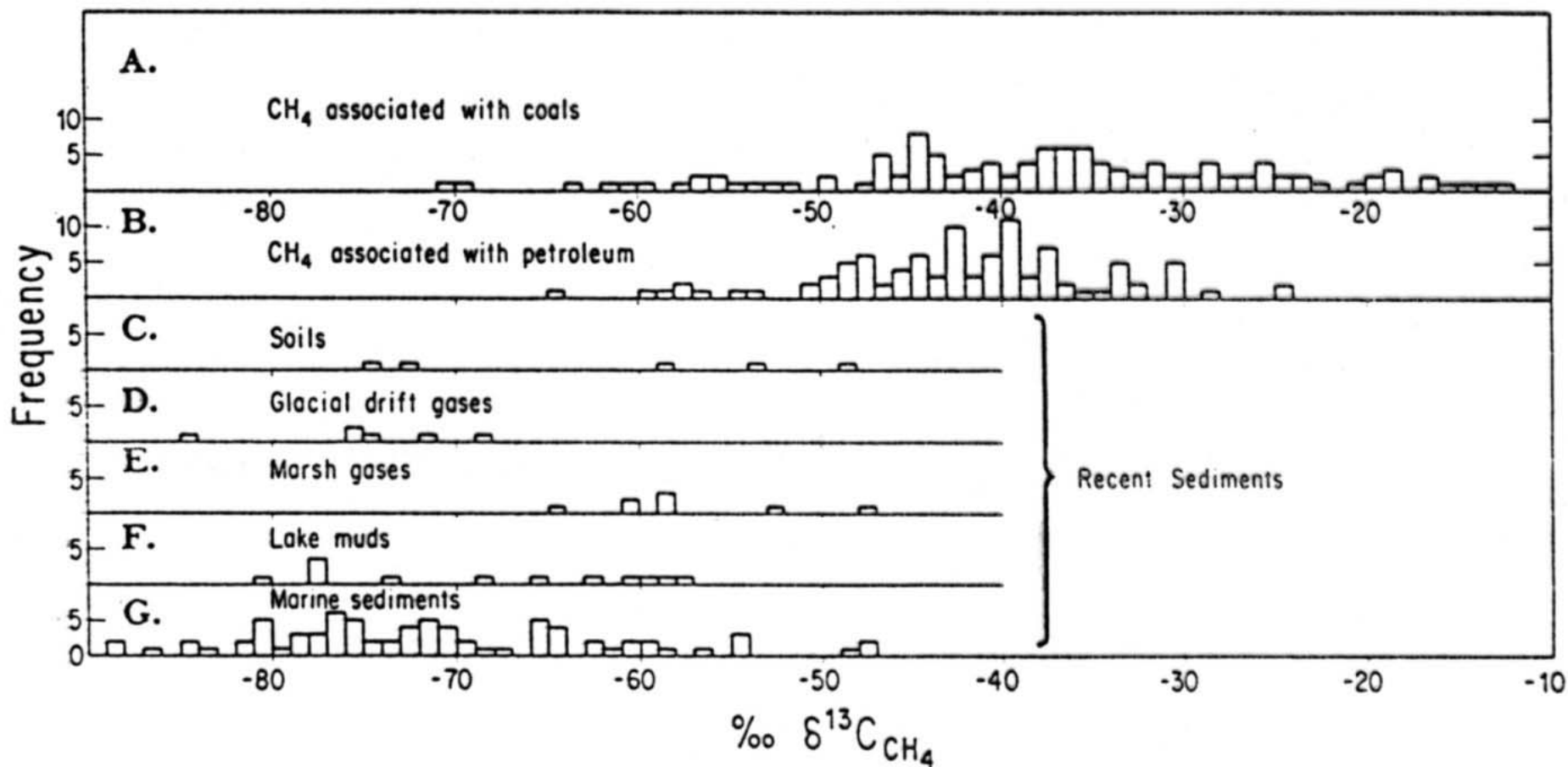
Fig. 9-15. Carbon isotopic composition of CH_4 from various sources. A. Coal gases. B. Methane associated with petroleum. C. Soil gases. D. Glacial drift gases. E. Marsh gases. F. Lake sediments. G. Marine sediments. Data from Colombo et al. (1968, 1970a, b), Dubrova and Nesmelova (1968), Galimov (1969), Lebedev (1964), Lebedev et al. (1969), Oana and Deevey (1960), Silverman (1964a, b), Stahl (1968a, b), Teichmüller et al. (1970), Vinogradov and Galimov (1970), Wasserburg et al. (1963), and Fig. 9-12.